HHS Public Access

Author manuscript

Cell Rep. Author manuscript; available in PMC 2018 October 17.

Published in final edited form as:

Cell Rep. 2018 August 28; 24(9): 2261–2272.e5. doi:10.1016/j.celrep.2018.07.092.

Ret and Substrate-Derived TGF-β Maverick Regulate Space-Filling Dendrite Growth in *Drosophila* Sensory Neurons

Nina Hoyer[1], **Philip Zielke**[1], **Chun Hu**[1], **Meike Petersen**[1], **Kathrin Sauter**[1], **Robin Scharrenberg**[2], **Yun Peng**[3], **Charles C. Kim**[4], **Chun Han**[5], **Jay Z. Parrish**[3], and **Peter Soba**[1,6,*]

[1]Research Group Neuronal Patterning and Connectivity, Center for Molecular Neurobiology (ZMNH), University Medical Center Hamburg-Eppendorf, 20251 Hamburg, Germany

[2]Research Group Neuronal Development, Center for Molecular Neurobiology (ZMNH), University Medical Center Hamburg-Eppendorf, 20251 Hamburg, Germany

[3]Department of Biology, University of Washington, Seattle, WA 98195, USA

[4]Verily, Mountain View, CA 94043, USA

[5]Weill Institute for Cell and Molecular Biology, Department of Molecular Biology and Genetics, Cornell University, Ithaca, NY 14853, USA

[6]Lead Contact

Summary

Dendrite morphogenesis is a highly regulated process that gives rise to stereotyped receptive fields, which are required for proper neuronal connectivity and function. Specific classes of neurons, including *Drosophila* class IV dendritic arborization (C4da) neurons, also feature complete space-filling growth of dendrites. In this system, we have identified the substrate-derived TGF-β ligand *maverick* (*mav*) as a developmental signal promoting space-filling growth through the neuronal *Ret* receptor. Both are necessary for radial spreading of C4da neuron dendrites, and Ret is required for neuronal uptake of Mav. Moreover, local changes in Mav levels result in directed dendritic growth toward regions with higher ligand availability. Our results suggest that Mav acts as a substrate-derived secreted signal promoting dendrite growth within not-yet-covered areas of the receptive field to ensure space-filling dendritic growth.

In Brief

Hoyer et al. uncover a mechanism for space-filling dendrite growth *in vivo*. Substrate-derived TGF-β Maverick and the Ret receptor together regulate the dendrite growth and stability of

*Correspondence: peter.soba@zmnh.uni-hamburg.de.

AUTHOR CONTRIBUTIONS

Conceptualization, N.H. and P.S.; Methodology, N.H., C.C.K., J.Z.P., and P.S.; Formal Analysis, N.H., P.Z., R.S., C.C.K., J.Z.P., and P.S.; Investigation, N.H., P.Z., C. Hu, M.P., K.S., and P.S.; Writing – Original Draft, N.H. and P.S.; Writing – Review and Editing, N.H., C. Hu, C. Han, J.Z.P., and P.S.; Funding Acquisition, C. Han, J.Z.P. and P.S.; Resources, C. Han, Y.P., and J.Z.P.; Supervision, P.S

DECLARATION OF INTERESTS

The authors declare no competing interests.

DATA AND SOFTWARE AVAILABILITY

The accession number for the C4da neuron microarray data reported in this paper is GEO: GSE115500.

Drosophila sensory neurons. They show that Ret is required for uptake of Maverick, whose local levels determine dendrite growth preference.

Abstract

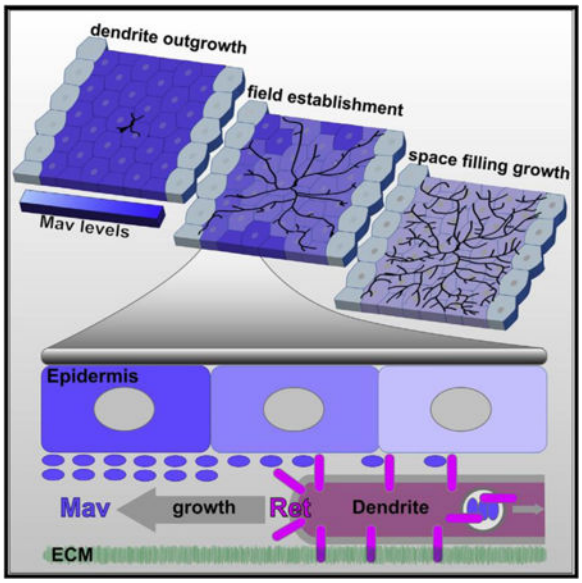

INTRODUCTION

Sensory perception relies on properly differentiated and connected neurons for accurate processing of inputs. Many neuronal classes establish subtype-specific, highly stereotyped dendritic branching patterns to cover their receptive field (Lefebvre et al., 2015). In addition, the dendritic fields of some types of neurons, including retinal ganglion cells and somatosensory neurons of both vertebrates and invertebrates, feature complete but non-redundant dendritic field coverage (Gallegos and Bargmann, 2004; Grueber et al., 2002; Sagasti et al., 2005; Wässle and Boycott, 1991). This phenomenon of space-filling dendrite growth and tiling requires even spreading of dendrites and, in the case of tiling, non-redundant partitioning of the innervated layer by dendrites of the same neuronal subtype. Although space-filling dendrite growth and tiling ensure proper synaptic or sensory input processing, it remains largely enigmatic how such complete field coverage is achieved during development.

The cell-intrinsic capacity to grow dendrites relies on specific transcriptional (Dong et al., 2015) and translational programs (Lin et al., 2015) that ensure sufficient growth capacity of neurons to acquire their defined subtype-specific morphology. Moreover, proper dendrite patterning is aided by like-repels-like mechanisms to ensure even and non-redundant receptive field formation. Prominently, self-avoidance is a major mechanism for recognition and repulsion of isoneuronal dendrites to prevent overlapping innervation (Zipursky and Grueber, 2013). In *Drosophila*, dendritic self-avoidance is mediated by the immunoglobulin superfamily member *Dscam* (Down syndrome cell adhesion molecule) through recognition and repulsion of isoneuronal dendrites (Hughes et al., 2007; Matthews et al., 2007; Soba et

al., 2007). In vertebrates, clustered protocadherins serve a similar function in space-filling neurons, including retinal ganglion and Purkinje cells (Lefebvre et al., 2012).

In addition to intrinsic programs, extrinsic cues and substrate interactions direct dendrite orientation, growth, and layering *in vivo*, with accumulating evidence showing that several molecular pathways contribute to neuronal subtype-specific layering and receptive field formation (Dong et al., 2015). One of the best studied models is *Drosophila* larval class IV dendritic arborization (C4da) neurons, which grow space-filling sensory dendrites and tile the entire body wall (Grueber et al., 2002). C4da neuron dendrites are normally confined to a 2-dimensional space on the basal face of the epidermis, where dendrites interact with the monolayer of epithelial cells and their underlying extracellular matrix (ECM) (Han et al., 2012; Kim et al., 2012b). Loss of integrin function leads to dendrite-ECM adhesion defects and results in dendrite embedding in the underlying epidermis. Therefore, integrins are essential to ensure repulsion-mediated self-avoidance, which restricts the growth of dendrites competing for the same territory. Similarly, loss of neuronal *plexB* or epithelial *sema2b* results in dendrite-ECM adhesion and self-avoidance defects in C4da neurons (Meltzer et al., 2016). Although dendrite-ECM adhesion ensures 2-dimensional growth required for dendrite self-encounters, loss of dendrite adhesion itself does not severely affect dendritic space-filling.

One candidate for regulation of space-filling growth and non-redundant dendrite patterning of C4da neurons is the conserved receptor tyrosine kinase *Ret* (re-arranged during transfection), which has been implicated in dendrite adhesion and stability in this system (Soba et al., 2015). Ret physically interacts with integrins to support C4da neuron dendrite-ECM adhesion via Rac1 signaling. In mammals, Ret signaling is believed to largely rely on binding of glial cell line-derived neurotrophic factor (GDNF) family ligands and the corresponding GDNF family co-receptors (Ibáñez, 2013). Although Ret is highly conserved in *Drosophila* (Hahn and Bishop, 2001; Hernández et al., 2015; Soba et al., 2015; Sugaya et al., 1994), GDNF homologs have not yet been identified in flies. The closest homologs found for GDNF are transforming growth factor β (TGF-β) family ligands, which comprise a large family of ancestral cysteine knot signaling molecules involved in diverse developmental and cellular pathways (Peterson and O'Connor, 2014; Saarma, 2000). Moreover, neither the *Drosophila* GFRα homolog *Gfrl* (Kallijärvi et al., 2012) nor integrins or *rac1* seem to play a role in *Ret*-dependent dendrite stability and growth defects of C4da neurons (Soba et al., 2015), suggesting that alternative interactors are involved in Ret-dependent dendrite patterning.

Here we have identified the TGF-β ligand *maverick* (*mav*) as an upstream mediator of *Ret* function, revealing a mechanism by which epidermis-derived Mav controls C4 da neuron radial dendrite spreading and space-filling growth.

RESULTS

The TGF-β Ligand Maverick Affects Ret-Dependent C4da Neuron Dendrite Development

To assess a potential role of TGF-β ligands, the closest homologs of GDNF in *Drosophila* (Saarma, 2000), in C4da neuron dendrite development, we overexpressed dActivin (dAct),

Dawdle (Daw), Glass-bottom boat (Gbb), Myoglianin (Myo) or Mav in C4da neurons or the larval body wall epidermis (*ppk-CD4-tdTomato; A58-Gal4*) (Figure S1A and data not shown). Only epithelial overexpression of Mav induced a strong C4 da neuron dendrite phenotype, resulting in increased dendrite length, terminal numbers, and abnormal field organization (Figures 1A–1E). To test whether this effect depended on *Ret*, we generated a knockout allele (Ret^{ko}; Figures S1B–S1E; see STAR Methods for details) using improved ends-out homologous recombination (Huang et al., 2009). Anti-Ret immunoreactivity in C4 da neurons was completely absent in Ret^{ko} animals, suggesting that it was indeed a null allele (Figures S1D and S1E). C4da neurons in Ret^{ko} animals displayed decreased dendrite coverage, dendrite length, and terminal numbers but increased dendrite crossing (Figures 1A–1E), phenocopying a previously reported hypomorphic *Ret* allele (Soba et al., 2015). If epidermal Mav signals through Ret to regulate dendrite growth, we predicted that mutation of *Ret* would block the growth-promoting activity of epithelial Mav overexpression. This is precisely what we found (Figures 1A–1E). Because endogenous *Ret* expression in the body wall is limited to C4da neurons (Figure S1D; Soba et al., 2015), these results show that *Ret* is epistatic to Mav, suggesting *mav* acts upstream of *Ret* in C4da neuron dendrite development.

We next investigated *mav* expression in the body wall during larval stages using a Minos Mediated Integration Cassette (MIMIC)-based GFP reporter ($mav^{Mi05038}$; Venken et al., 2011) inserted in *mav* exon 1 close to the translational start (Figure 1F). The reporter signal could be visualized from 48 hr AEL (after egg laying) onward, showing epithelial but not neuronal expression in the larval body wall (Figure 1G; Figure S1F). Similarly, a genomic fosmid transgene containing a GFP-tagged *mav* ($mav\text{-}GFP^{Fos}$; Sarov et al., 2016) displayed low-level epithelial expression of Mav-GFP (Figures 1F and1H).

These results show *Ret*-dependent action of epithelial Mav on C4da neuron dendrite morphogenesis. Moreover, endogenous Mav is expressed in the larval body wall epithelium within the expanse of C4da neuron dendritic fields.

Mav and Ret Are Similarly Required for C4da Neuron Radial Dendrite Growth and Field Coverage

We next probed the requirement of endogenous *mav* in dendrite growth and compared it with *Ret* function. RNAi-mediated knockdown of *mav* specifically in the body wall epithelium led to decreased dendrite length, coverage, and complexity of C4da neurons (Figures S1G–S1J), showing that epidermal mav is required to support C4da dendrite growth. We then generated a *mav* loss of function allele using the CRISPR/Cas9 system (Gratz et al., 2013; Port et al., 2014), replacing *mav* coding exons with a marker cassette by homology-directed repair (mav^{ko}; Figures S2A and S2B). Similar to Ret^{ko}, mav^{ko} animals were viable, fertile, and exhibited morphological defects in C4da neurons (Figure 2A). Prominently, *mav* and *Ret* were required for proper radial distribution of dendritic arbors because their loss of function resulted in preferential dendritic growth along the anterior to posterior and dorsal-ventral (d/v) axes. We generated qualitative heatmaps for dendrite distribution by registering and overlaying multiple *Ret* and *mav* mutant C4da neurons illustrating the shift in highest dendrite coverage to axial portions (anterior to posterior and

d/v axes) of the receptive field (n = 5; Figure 2B). Quantitative analyses of dendritic distribution confirmed that *mav* and *Ret* function were required for radial dendrite organization (Figure 2B'). Moreover, C4da neurons in mav^{ko} or Ret^{ko} mutant larvae exhibited similarly reduced dendrite length, terminal numbers, and dendritic complexity (Figures 2C–2E).

Previous analyses have uncovered aspects of *Ret* function that are integrin-dependent (dendrite crossing and ECM adhesion) and -independent (dendrite stability; Soba et al., 2015). Mav^{ko} and Ret^{ko} mutant larvae both displayed C4da neuron dendrite crossing and ECM detachment defects, suggesting that they are similarly involved in integrin-dependent functions (Figures S2C and S2D).

We then compared developmental C4da neuron dendrite turn-over between 72 hr and 96 hr AEL in mav^{ko} or Ret^{ko} mutant larvae using time-lapse microscopy. The loss of either *mav* or *Ret* resulted in increased dendritic growth and retraction within this 24-hr time frame, with the overall growth rate being reduced to 50% of controls (Figures S2E–S2G). To assess the temporal re-quirements for *mav* in C4da dendrite growth, we monitored the onset of dendrite growth defects in mav^{ko} larvae during development. Dendritic coverage and crossing defects were evident at 48 hr AEL, a time point when control C4da neurons displayed complete receptive field innervation (Figures S2H– S2K). However, dendritic growth defects were first evident at 72 hr AEL. This suggests an early requirement for *mav* in receptive field establishment as well as an ongoing requirement for dendrite growth and branching, resulting in progressive failure of receptive field coverage.

Taken together, our comprehensive analysis of *mav* and *Ret* loss of function phenotypes revealed that both are similarly required for C4da neuron dendrite growth, distribution, complexity, and stability as well as ECM adhesion and dendrite crossing.

Mav Functions Upstream of Ret in C4da Neuron Development

To further investigate the epistatic relationship of *Ret* and *mav*, we compared the phenotypes of C4da neurons lacking *mav* function, *Ret* function, or both. We found that the morphological defects of C4da neurons in mav^{ko}, Ret^{ko}, and Ret^{ko}+mav^{ko} animals were indistinguishable from one another but significantly different from controls (Figures 3A–3D).

Because *mav* likely functions upstream of *Ret*, reintroducing the *mav* genomic region using a bacterial artificial chromosome (BAC) transgene (mav^{DP}) should rescue mav^{ko} but not Ret^{ko} and *Ret+mav* double mutant phenotypes. As anticipated, mav^{DP} partially rescued dendrite growth defects and terminal numbers in mav^{ko} but not in Ret^{ko} or Ret^{ko}+mav^{ko} double mutant animals (Figures 3A–3D).

Conversely, overexpression of the putative receptor Ret might restore some aspects of dendrite development in Ret^{ko}/mav^{ko} animals because of auto-activation, even in the absence of a ligand. Overexpression of Ret in C4da neurons of Ret^{ko}/mav^{ko} animals indeed partially rescued dendrite growth defects but could not restore normal dendrite distribution, terminal numbers, or crossing (Figures S3A–S3D). To assess whether canonical TGF-β

receptors play a role in *mav*-mediated dendrite development, we analyzed mutant alleles of all known type I and II receptors but did not find any significant effects on C4da neuron dendrites (Figure S3E).

Taken together with our finding that *Ret* mutation is epistatic to epidermal Mav overexpression (Figures 1A–1E), these data show that *mav* acts upstream of *Ret* and likely independent of classical TGF-β receptors to regulate C4da neuron dendrite patterning.

Ret Receptor Function in C4da Neuron Dendrite Development Requires Its Extra- and Intracellular Domain

We next set out to characterize Ret domains required for its function, focusing on the conserved N-terminal Cadherin-like domain (CLD), cysteine-rich domain (CRD), and its intracellular tyrosine kinase domain (Figure 4A; Ibáñez, 2013). We created Ret transgenes lacking extra- and intracellular domains or carrying a point mutation that impaired kinase activity (Ret^{K805M}; Abrescia et al., 2005) and assessed their ability to rescue C4da neuron dendrite development in *Ret* mutant animals.

As a control, we first expressed a full-length Ret transgene in C4da neurons and found that it could completely rescue dendrite defects of Ret^{ko} mutants, including total dendrite length, number of crossing points, dendrite-ECM adhesion, and branching complexity (Figures 4B, 4D–4G, and S4E). In contrast, expressing *Ret* lacking either the extra- or intracellular domain did not alleviate these defects (Figures 4A–4G and S4E). Surprisingly, expressing a kinase-dead variant (Ret^{K805M}) or Ret lacking the entire kinase domain still exhibited significant rescue activity, although the latter could not fully restore dendrite length and branch complexity (Figures 4C, 4D, and 4G), suggesting that its kinase function might not play a major role in C4 da neuron dendrite development.

Although C4da neuron-specific overexpression of these Ret transgenes had no major effect on dendrite morphology, we noticed that ectopic expression of Ret in all sensory da neurons or in the posterior epidermal compartment strongly interfered with the growth of C4da neuron dendrites into the ectopic Ret expression domain (Figures S4A–S4D). This effect was fully dependent on Ret extra- but not intra-cellular domains, suggesting that cell surface interactions of ectopic Ret prevent normal C4da neuron dendrite development. These findings suggest that ectopic Ret competes for a limited ligand pool, potentially by acting as a sponge for Mav and other factors.

To test whether Ret and Mav are also sufficient to promote dendrite growth, we expressed both ectopically in C1da (*nompC-Gal4*) or C3da neurons (*19–12-Gal4*), which endogenously express neither Ret nor Mav. Dendrite growth and branching of C1da neurons were significantly enhanced by co-overexpression of Ret and Mav but not Ret or Mav alone (Figures S5A–S5C). However, truncated forms of Ret in combination with Mav did not significantly alter C1da neuron dendrites, suggesting that the extra- and intracellular domain of Ret are necessary for Mav-dependent dendrite growth. Similarly, co-overexpression of Ret and Mav in C3da neurons was able to strongly increase their dendrite coverage (Figures S5D and S5E).

To gain insight into downstream effects of Ret signaling, we performed microarray analyses of purified control and *Ret*^{ko} C4da neurons. We identified 64 genes that were significantly differentially expressed in *Ret*^{ko} C4da neurons, including 36 up- and 28 downregulated ones (Figures S6A–S6C). Functional classification of the deregulated genes revealed that a significant subset of candidate genes is involved in cellular and metabolic signaling (Figures S6A–S6C). Although we could not link these candidates to known Ret signaling components, some of the affected genes, including *vis* (Wang and Mann, 2003), *RanBPM* (Zhang et al., 2014), and *CG8768* (Kim and Marqués, 2010), have previously been implicated in TGF-β signaling.

Overall, our structure-function analysis shows that Ret function in C4da neuron development requires both its extra- and intracellular domains. Moreover, Ret and Mav together are sufficient to promote dendrite growth and branching, suggesting a common downstream signaling mechanism potentially identified by our microarray analysis.

Epithelial Mav Levels Direct C4da Neuron Dendrite Growth Preference

We hypothesized that epidermal cells act as a Mav-dependent growth substrate for C4da neurons, which promotes dendrite growth into areas with higher Mav levels.

We tested this by overexpression of *UAS-mav* (*mav*^{OE}) or *UAS-mav-RNAi* (*mav*^{RNAi}) only in the posterior (*engrailed-Gal4* [*en-Gal4*]) or dorsal (*ushaped-Gal4* [*ush-Gal4*]) epithelial compartment of the C4da neuron dendritic field.

Overexpression of Mav with *en-Gal4* strongly enhanced dendrite growth of C4da neurons into the *en-Gal4* domain while reducing growth in the anterior compartment (Figure 5A). Conversely, RNAi-mediated knockdown of Mav within the *en-Gal4* domain resulted in a 2-fold local reduction of C4da neuron dendrites with a concomitant 2-fold increase in dendrites covering the anterior field. Intriguingly, total dendrite length was not affected by either manipulation (Figures 5B–5D).

We obtained virtually identical results by manipulating Mav levels in the dorsal part of the C4da neuron-receptive field using *ush-Gal4* (Figures S6D–S6G). In this case, reduction of Mav levels by RNAi resulted in a 2-fold shift of preferential dendrite growth into the ventral domain, whereas overexpression of Mav led to a more than 2-fold increase in dendrites covering the dorsal field.

Together, these results show that local epidermal Mav expression levels regulate the dendrite growth preference of C4da neurons, biasing dendrite growth toward regions with higher Mav expression.

Ret Is Required for Neuronal Uptake of Mav

We next investigated the relationship between Mav protein distribution and abundance and neuronal Ret. We took advantage of the genomic *mav-GFP*^{Fos} transgene, which displayed specific Mav-GFP protein expression in the body wall epithelium and partial rescue activity of C4da neuron morphology in *mav*^{ko} animals (Figures 1H and S7A–S7E). In controls, low levels of Mav-GFP could be detected in punctate structures associated with epithelial cells

(Figures 5E and S7F). However, *Ret*^{ko} mutant animals displayed strongly increased Mav-GFP levels in epithelial cells, which could be reduced to below control levels upon Ret overexpression in C4da neurons. These findings suggest that the presence of *Ret* in C4 da neurons regulates epithelial Mav levels.

To test the possibility that epithelial Mav levels might be regulated by Ret-dependent internalization into C4 da neurons, we generated a *UAS-2xHA-mav* transgene containing a tandem hemagglutinin (HA) tag for increased sensitivity and overexpressed 23HA-Mav exclusively in the epithelium. Indeed, we detected punctate structures of Mav specifically in proximal and distal dendrites of C4 da neurons (Figures 5F–5F’’). Mav puncta in C4da neurons were completely absent in *Ret*^{ko} animals and were undetectable when we omitted detergent during immunostaining, suggesting that Mav can be internalized by C4da neurons in a *Ret*-dependent manner (Figures 5G and5H and data not shown). Together, these data show that epithelium-derived Mav protein levels are likely regulated by Ret-dependent neuronal uptake.

Epithelial Mav Is Secreted and Can Diffuse across the Body Wall Epithelium

Because most TGF-β ligands are secreted, we wanted to assess Mav localization upon local expression. To this end, we overexpressed 2×HA-Mav in the posterior part of the epithelium using *en-Gal4* and assessed total and cell surface distribution of Mav. Similar to non-tagged Mav, 2×HA-Mav expression with *en-Gal4* resulted in preferential C4da neuron dendrite growth in the posterior part of the receptive field (Figure 6A). Accordingly, total 2×HA-Mav levels were high in the *en-Gal4* domain and rapidly declined anterior to the expression domain (Figures 6A’ and 6B). As before, we detected a neuronal Mav signal in C4da neurons upon 2×HA-Mav expression but not in controls, suggesting Mav can be internalized by dendritic uptake (Figure S7G). In contrast, omitting detergent treatment (no TX-100) during immunostaining revealed widespread Mav localization along the basal epithelial surface within the entire C4da neuron dendritic field (Figures 6C and6D). No obvious Mav signal was detected in C4da neuron dendrites under these conditions (Figure S7G). These data suggest that epidermis-derived Mav is secreted and can diffuse locally within the expanse of the C4da neuron receptive field.

Epithelial Mav Acts Locally and Proximally to Promote C4da Neuron Dendrite Growth

To assess whether Mav acts locally or at a distance to control C4da neuron dendrite growth, we used epithelium-specific Flipase (Flp) transgenes to generate either low-frequency (LF-Flp) or high-frequency (HF-Flp) Gal4-expressing epithelial clones (*actin- > FRT > y*$^{+}$ *> FRT > Gal4*).

First we assessed the distribution of surface Mav by expressing 2×HA-Mav in LF-Flp epithelial clones. Although control immunostainings showed no specific signal (Figures 7A, 7A’, and 7A’’), we detected low levels of surface Mav typically lining a portion of a C4 da neuron dendrite crossing the epithelial clones (Figures 7B and7B’). Overexpression in this case was significantly lower than when we constitutively overexpressed *mav* with *en-Gal4*, and we found that Mav surface levels on epithelial clones at sites without dendrite contact were low (Figure 7B’’). Furthermore, Mav did not accumulate to detectable levels on the

cell surface outside of the clones, demonstrating that the LF-Flp system allows for local modulation of Mav levels.

We then tested how downregulation or overexpression of Mav in subsets of epithelial cells would affect dendrite coverage. Overexpression of Mav in few epithelial cells (LF-Flp > mav^{OE}) re-sulted in strong rearrangement of C4da neuron dendrite growth (Figures 7C and7E). Interestingly, Mav overexpression not only caused increased dendrite coverage of Mav-expressing epithelial clones (Figure 7C, green areas) but also induced increased dendrite growth in surrounding areas (red area surrounding epithelial clones) while decreasing coverage in more distant areas.

In turn, RNAi-mediated downregulation of Mav in few epithelial cells (LF-Flp > mav^{RNAi}) resulted only in a local reduction of dendrite coverage of epithelial clones but not surrounding cells (Figures 7C and7E). These data indicate that reduction of Mav levels in few epithelial cells impairs C4da neuron dendrite coverage only locally on the affected epithelial cells, whereas Mav overexpression increases dendrite coverage of epithelial clones and surrounding cells.

We then induced high-frequency epithelial mosaics (HF-Flp) expressing mav^{RNAi} to test whether Mav expression in the remaining non-expressing epithelial cells was sufficient to maintain local dendrite coverage. Reduction of Mav expression in most epidermal cells resulted in a global reduction of dendrite coverage: even non-expressing epithelial cells (shaded red area) displayed the same reduced dendrite coverage as Mav-RNAi-expressing cells (Figures 7D and7F).

Consistent with the idea that Mav is secreted, these findings show that Mav supports dendrite growth locally and at a distance, whereas Mav expression in only few cells is not sufficient to maintain local or global dendrite coverage.

DISCUSSION

Ret and Mav Function in a Common Pathway in C4da Neuron Development

Our findings show that the TGF-β ligand Mav acts as a Ret-dependent growth cue regulating C4da neuron dendrite spreading to ensure space-filling dendrite coverage. TGF-β ligands are evolutionary conserved signaling modules present in all metazoans and the closest conserved homologs of the mammalian GDNF family (Peterson and O'Connor, 2014; Saarma, 2000). So far, only activin has been implicated in the regulation of dendritic organization by restricting dendritic field size of amacrine cells through TGF-β signaling (Ting et al., 2014), whereas *Mav* can act as a glial-derived cue regulating neuromuscular junction (NMJ) growth (Fuentes-Medel et al., 2012). *Mav* displays limited homology to both bone morphogenetic protein (BMP) or activin-like ligands (Nguyen et al., 2000), with the highest homology to mammalian GDF-15.

Our genetic data show that *mav* acts upstream of *Ret* in space-filling dendrite growth. First, Mav function in dendrite growth and patterning requires the presence of Ret. Second, epithelial Mav protein levels were increased in the absence of neuronal *Ret.* Third,

epithelium-derived Mav is internalized by C4da neurons in a *Ret*-dependent manner. Taken together, these data suggest that signaling required for space-filling dendrite growth is likely elicited by Ret-mediated neuronal up-take of Mav.

Recent work showed that the mammalian Mav homolog GDF-15 and the GDNF family receptor α-like (GFRAL) are a high-affinity ligand-receptor pair. Intriguingly, the GFRAL/GDF-15 complex signals through Ret in the mammalian brain stem to mediate GDF-15-dependent anti-obesity effects (Emmerson et al., 2017; Hsu et al., 2017; Mullican et al., 2017; Yang et al., 2017). In *Drosophila*, *Ret*, *mav*, and the GFR-like co-receptor form a biochemical complex and function in stomatogastric nervous system development (Myers et al., 2018). Thus, it seems plausible that Mav and Ret form a functional signaling pair here too, although neither GFRL nor classical TGF-β receptors play a role in space-filling dendrite growth of C4da neurons. Moreover, although *Drosophila* Ret has tyrosine kinase activity, which is required in other contexts (Abrescia et al., 2005; Perea et al., 2017), our findings suggest that it might play a lesser role in C4da neuron dendrite patterning. Thus, Ret function in this system likely requires additional co-receptors. Notably, Ret is able to form functional complexes with several cell surface molecules, including integrins (Soba et al., 2015), vascular endothelial growth factor (VEGF) (Tufro et al., 2007), TrkB (Esposito et al., 2008), and Eph/Ephrin (Bonanomi et al., 2012; Kramer et al., 2006), suggesting that it acts as a modular signal transducer. Based on our genome-wide analysis, Ret also regulates the expression levels of a small subset of signaling molecules, which are likely involved in downstream responses. This provides an entry point to identify the precise co-receptor and downstream signals required for Ret and Mav function in dendritic space-filling.

Mav Promotes Dendrite Space-Filling via Ret

In our study, we showed that Mav is expressed and localized in the larval body wall epithelium covering the receptive field expanse of C4da neurons. Loss of *mav* or neuronal *Ret* alters C4da neuron dendrite patterning from radial to axial growth, leaving significant portions of the receptive field uncovered. Thus, although axial growth cues might still be present, *mav* and *Ret* are critical for radial spreading and complete coverage of C4da neuron dendrites. This suggests that Mav is a substrate-derived cue determining receptive field shape and coverage. Besides Ret and Mav, *Tenascin-M* has been shown to be required for radial growth of high-order dendrites (Hattori et al., 2013), suggesting that additional signaling pathways might regulate the final radial shape of C4 da neuron dendrites. Indeed, emerging evidence suggests that substrate-derived ligands and adhesion play a major role in dendrite development, which is orchestrated by multiple cell surface cues (Dong et al., 2015; Le-febvre et al., 2015). In *Drosophila* C4da neurons, Ptp69D is required for normal dendritic growth and coverage (Poe et al., 2017), whereas the protocadherin *flamingo* and the transmembrane protein *golden goal* are necessary to prevent dorsal dendrite overextension (Gao et al., 2000; Hakeda and Suzuki, 2013; Matsubara et al., 2011). Moreover, the α-integrin *mew*, β-integrin *mys* (Han et al., 2012; Kim et al., 2012b), and *PlexB/ Sema2b* (Meltzer et al., 2016) are required for 2-dimensional growth and ECM adhesion of sensory neuron dendrites. *Ret* has previously been shown to interact with integrins and Rac1 in C4 da neurons to promote dendrite-ECM adhesion and, thus, a 2-dimensional growth mode (Soba et al., 2015). Consistently, our results show that C4da neurons in *Ret* and *mav* mutant

animals also display dendrite-ECM adhesion defects, resulting in dendrite crossing, suggesting that *mav* and integrin function are linked via Ret. However, Ret and Mav also display a unique role in C4da neuron dendrite space-filling because their absence leads to increased dendrite turnover and failure to stabilize growing dendrites, resulting in incomplete receptive field coverage. This suggests that Mav, through Ret, stimulates integrin/Rac1-dependent ECM adhesion and, independently, dendrite growth stabilization required for space-filling.

Similarly, dendritic fields are shaped by substrate interaction in other model organisms as well. In *C. elegans*, Sax-7 forms a subcellular pattern in the hypodermis and, together with mnr-1, provides the substrate required for patterning of PVD dendrites via the neuronal receptor DMA-1 (Dong et al., 2013; Liu and Shen, 2011; Salzberg et al., 2013). In mouse, ON starburst amacrine cells (SACs) expressing both PlexA2 and Sema6A form radially symmetric dendritic fields, which requires PlexA2/Sema6A repulsive action (Sun et al., 2013). Interestingly, Ret regulates the function and morphology of retinal ganglion cells (Brantley et al., 2008), which also express GDF-15 (Charalambous et al., 2013), indicating a possible common function in this system.

Mav Distribution and Levels Direct Dendritic Field Growth

Our experimental evidence suggests that C4da neuron dendrite growth and stability is promoted by local abundance of epithelial Mav. C4da neuron dendrites occupied areas with higher Mav expression levels after local up- or downregulation of Mav. Moreover, Mav-overexpressing epithelial clones resulted in a local increase in dendrite occupancy, consistent with growth stabilization depending on Mav abundance. Conversely, reduction of Mav levels in few epithelial cells resulted in locally reduced dendrite coverage, whereas widespread depletion of Mav in most epithelial cells led to dendrite coverage defects even in non-manipulated regions. Overall, these results are highly consistent with Mav acting as a secreted short-range growth cue.

Our developmental analysis of C4da neurons in mav^{ko} animals and local Mav overexpression data provide evidence that Mav acts very early during initial field establishment, where growth is preferentially increased and stabilized within and close to the source of higher Mav expression. Our results further suggest that extracellular Mav levels are kept very low under physiological conditions, likely by Ret-mediated uptake into C4da neurons. This is consistent with ectopic Ret overexpression in other sensory neurons disrupting C4 da neuron development, which are then competing for Mav. Conversely, Ret and Mav co-expression in C1da or C3da neurons was sufficient to promote their growth, possibly by strong cell-autonomous induction of Mav/Ret signaling. Intriguingly, recent evidence showed that the heparan sulfate proteoglycans (HSPGs) Dally and Syndecan are synergistically required in epithelial cells to locally stabilize extending C4 da neuron dendrites, rendering the environment permissive for growth (Poe et al., 2017). It is possible that Mav requires HSPGs for extra-cellular spreading and function, consistent with the importance of HSPGs in TGF-β gradient formation and function across species (Yan and Lin, 2009).

Based on our data, we hypothesize that, during dendritic field establishment, epithelial Mav provides a growth-stabilizing cue promoting radial and even extension of C4da neuron dendrites. Local extracellular Mav might elicit Ret-dependent neuronal uptake and signaling in dendrites extending into that area, stabilizing growth but reducing local Mav levels. In turn, epithelial cells not yet covered by C4da dendrites provide a local source of higher extracellular Mav concentration, promoting growth into this region until the entire substrate is evenly covered and Mav levels are uniform (Figure S7H). Consistent with our data, such a mechanism would ensure uniform space-filling coverage of the entire receptive field of C4da neurons. Our findings open the possibility that similar substrate or target cell-derived growth-regulating mechanisms are operating in other systems.

STAR★METHODS

KEY RESOURCES TABLE

REAGENT or RESOURCE	SOURCE	IDENTIFIER
Antibodies		
guinea-pig anti-Ret	provided by I. Miguel-Aliaga, Soba et al., 2015	N/A
rabbit anti-GFP	ThermoFisher	Cat#A11122 RRID: AB_221569
mouse anti-coracle C615.16	DSHB, Iowa	SHB Cat# C615.16, RRID:AB_1161644
rat anti-HA, clone 3F10	Roche	Roche Cat# 11867423001, RRID:AB_10094468
Cy3 AffiniPure Donkey Anti-Guinea Pig IgG (H+L)	Jackson ImmunoResearch, Westgrove, PA	Cat# 706–165-148 RRID:AB_2340460
DyLight 488 AffiniPure Donkey anti Rabbit IgG (H+L) antibody	Jackson ImmunoResearch, Westgrove, PA	Cat# 711–485-152 RRID:AB_2492289
Cy3 AffiniPure Donkey Anti-Mouse IgG (H +L)	Jackson ImmunoResearch, Westgrove, PA	Cat# 715–175-151 RRID: AB_2340820
Cy5 AffiniPure Donkey Anti-Rat IgG (H+L)	Jackson ImmunoResearch, Westgrove, PA	Cat# 712–165-153 RRID: AB_2340672
Alexa Fluor 647 AffiniPure Goat Anti-Horseradish Peroxidase	Jackson ImmunoResearch, Westgrove, PA	Cat# 123–605-021 RRID: AB_2338967
Critical Commercial Assays		
RNAqueous Micro kit	ThermoFisher	Cat#AM1931
Aminoallyl MessageAmp II kit	ThermoFisher	Cat#AM1753
Deposited Data		
Microarray analysis of *Ret^{ko}* C4da neurons	This study	NCBI Gene Expression Omnibus (GEO: GSE115500)
Experimental Models: Organisms/Strains		
D. melanogaster: *Ret^{C168}:* PBac{3HPy^{+}}Ret^{C168}	Soba et al., 2015	N/A
D. melanogaster: *Df(2L)Bsc^{312}*: w[1118]; Df(2L)BSC312/CyO	Bloomington Drosophila Stock Center	RRID: BDSC_24338

REAGENT or RESOURCE	SOURCE	IDENTIFIER
D. melanogaster: *ppk-CD4-tdTomato*: w[1118]; P{w[+mC] = ppk-CD4-tdTom}10a/TM6B, Tb[1]	Han et al., 2011	RRID: BDSC_35845
D. melanogaster: *ppk-CD4-tdGFP*: w[1118]; P{w[+mC] = ppk-CD4-tdGFP}8/TM6B, Tb[1]	Han et al., 2011	RRID: BDSC_35843
D. melanogaster: *ppk-Gal4*: w[1118]; P{w[+mC] = ppk-Gal4} /TM6B, Tb[1]	Han et al., 2011	N/A
D. melanogaster: *UAS-CD4-tdGFP*: w[1118]; PBac{y[+mDint2] w[+mC] = UAS-CD4-tdGFP}VK00033	Han et al., 2011	RRID: BDSC_35836
D. melanogaster: *trol-GFP*: P{PTT-un1}trolG00022	Soba et al., 2015	N/A
D. melanogaster: *19–12-Gal4*: w[1118]; P{w[+mC] = 19–12-Gal4} /TM6B, Tb[1]	Yan et al., 2013	N/A
D. melanogaster: *UAS-CD4-tdTomato*: w[1118]; PBac {y[+mDint2] w[+mC] = UAS-CD4-tdTom}VK00033	Han et al., 2011	RRID: BDSC_35837
D. melanogaster: *A58-Gal4*	Jiang et al., 2014	N/A
D. melanogaster: *pzk-Flp1*	Poe et al., 2017	N/A
D. melanogaster: ush-Gal4: w[*]; P{w[+mW.hs] = GawB} NP0022 / CyO, P{w[-] = UAS-lacZ.UW14}UW14	DGRC Kyoto	DGRC #103497
D. melanogaster: *mav-GFP*^{Fos}	Sarov et al., 2016	VDRC #318248
D. melanogaster: *nompC-Gal4*: w[1118]; P{y[+t7.7] w[+mC] = GMR41E11-GAL4}attP2	Bloomington Drosophila Stock Center	RRID: BDSC_50131
D. melanogaster: *en-Gal4*: y[1] w[*]; P{w[+mW.hs] = en2.4-GAL4}e16E	Bloomington Drosophila Stock Center	RRID: BDSC_30564
D. melanogaster: *UAS-mav*$^{RNAi\{TRiP.GL01025\}attP40}$: y[1] sc[*] v[1]; P{y[+t7.7] v[+t1.8] = TRiP.GL01025}attP40	Bloomington Drosophila Stock Center	RRID: BDSC_36809
D. melanogaster: *UAS-mav*$^{RNAi\{TRiP.HMS01125\}attP2}$: y[1] sc[*] v[1]; P{y[+t7.7] v[+t1.8] = TRiP.HMS01125}attP2	Bloomington Drosophila Stock Center	RRID: BDSC_34650
D. melanogaster: *mav*^{MI05038}: y[1]; Mi{y[+mDint2] = MIC}mav [MI05038]	Bloomington Drosophila Stock Center	RRID: BDSC_60780
D. melanogaster: *UAS-gbb*	O'Connor lab	N/A
D. melanogaster: *UAS-dAct*	O'Connor lab	N/A
D. melanogaster: *UAS-daw*	O'Connor lab	N/A
D. melanogaster: *UAS-mav*	O'Connor lab	N/A
D. melanogaster: *UAS-myo*	O'Connor lab	N/A
D. melanogaster: *UAS-2xHA-mav:* w[1118]; P{w[+mW.hs] = UAS-2xHA-mav }attP2	This study	N/A
D. melanogaster: *UAS-Ret*: w[1118]; P{w[+mW.hs] = UAS-Ret-V5 }attP2	This study	N/A

REAGENT or RESOURCE	SOURCE	IDENTIFIER
D. melanogaster: *UAS-Ret-CTΔ*: w[1118]; P{w[+mW.hs] = UAS-Ret-CTD-V5 }attP2	This study	N/A
D. melanogaster: *UAS-Ret-NTΔ:* w[1118]; P{w[+mW.hs] = UAS-Ret-NTD-V5 }attP2	This study	N/A
D. melanogaster: *UAS-Ret-KDΔ*: w[1118]; P{w[+mW.hs] = UAS-Ret-KDD-V5 }attP2	This study	N/A
D. melanogaster: *UAS-Ret-K805M:* w[1118]; P{w[+mW.hs] = UAS-Ret-K805M-V5 }attP2	This study	N/A
Oligonucleotides		
See Table S1	This paper	
Software and Algorithms		
Fiji	https://fiji.sc/	RRID: SCR_002285
Origin Pro	Originlab Corp., Northampton, U.S.A.	N/A
Imaris Filament Tracer	BitPlane AG, Zurich,€ Switzerland	RRID: SCR_007366
AutoQuant	BitPlane AG, Zurich,€ Switzerland	RRID: SCR_002465

CONTACT FOR REAGENT AND RESOURCE SHARING

Further information and requests for resources and reagents should be directed to and will be fulfilled by the Lead Contact, Dr. Peter Soba (peter.soba@zmnh.uni-hamburg.de).

EXPERIMENTAL MODEL AND SUBJECT DETAILS

Fly strains and husbandry—All fly stocks were maintained at 25 C and 70% rel. humidity on standard cornmeal/molasses food. Staged male and female 3rd instar larvae (96h AEL) were used unless otherwise noted. All experiments were conducted on age- and size-matched larvae.

The following fly stocks were used: Ret^{C168}, $Df(2L)Bsc^{312}$ (deficiency covering the genomic Ret locus), *trol-GFP* (Soba et al., 2015), *ppk-CD4-tdTomato, ppk-Gal4, UAS-CD4-tdGFP, UAS-CD4-tdTomato*, (Han et al., 2011), low (LF-Flp) and high frequency (HF-Flp) epithelium-specific Flp lines (Poe et al., 2017), *A58-Gal4* (Jiang et al., 2014), *19–12-Gal4* (Yan et al., 2013), *nompC-Gal4* (*GMR41E11-GAL4,* BDSC #50131), *en-Gal4* (BDSC #30564), $mav\text{-}GFP^{Fos}$ (VDRC #318248), $UAS\text{-}mav^{RNAi\{TRiP.GL01025\}attP40}$ (BDSC #36809), $UAS\text{-}mav^{RNAi\{TRiP.HMS01125\}attP2}$ (BDSC #34650), $mav^{MI05038}$ (BDSC #60780), *ushaped* (*ush*)-$Gal4^{NP0022}$ (DGRC Kyoto #103497), *UAS-gbb, UAS-dAct, UAS-daw, UAS-mav, UAS-myo* (kindly provided by T. Haerry and M. O'Connor).

Plasmids of full length, truncated, and mutated Ret cDNA constructs carrying a C-terminal V5 tag (CTΔ, NTΔ, KDΔ, K805M) and 2xHA-tagged Mav (internal 2xHA tag inserted at

position 341 of the Mav protein sequence) were generated by PCR-amplification and cloned into pUAST-AttB (see Table S1). Transgenes were generated by embryo injection using *vasa-ΦC31;attP2* carrying flies (Groth et al., 2004).

Construction of transgenic and knockout animals—A *Ret* knockout allele (Ret^{ko}) was generated by an improved ends-out genomic targeting strategy (Huang et al., 2009). Exons 3–8 (E3–8) were replaced by a targeting cassette with 5′ (5kb) and 3′ (3kb) homologous regions flanking a GMR-white cassette (Table S1). Red eyed *Ret* mutant candidates were validated by PCR using primers flanking the GMR cassette and 5′ and 3′ targeting site in the Ret genomic locus to verify correct gene replacement. Out of three correctly targeted lines, Ret^{ko} line 2.7 was selected for all further experiments based on viability, total loss of anti-Ret immunoreactivity and fully rescuable C4 da neuron dendrite phenotypes.

A *mav* knockout (mav^{ko}) allele was generated by CRISPR/Cas9-mediated homology directed repair (HDR) (Gratz et al., 2013; Port et al., 2014). Guide RNAs targeting the 5′ and 3′ ends of the *mav* coding exons 2 and 3 on the 4th chromosome were cloned into pCFD4 (Table S1) to express both under control of the U6–1 and U6–3 promoter, respectively. pRK2 (Huang et al., 2009) was used to generate an HDR donor template containing 1kb genomic DNA up- and downstream of the *mav* coding exons. Both plasmids were co-injected into *yw,vasa-Cas9* syncytial embryos to target *mav* in the germline. mav^{ko} candidate animals were identified by eye color and correct targeting was verified by PCR analysis. One correctly targeted viable line (no.2) was selected for all subsequent experiments.

METHOD DETAILS

In vivo confocal microscopy—For live imaging 3rd instar larvae (96hrs AEL), C1da (ddaD), C3da (ddaA and ddaF) and C4da neurons (ddaC) were imaged by confocal microscopy (Zeiss LSM700) as previously described (Soba et al., 2015). C4 da neurons were visualized by using either *ppk-CD4-tdTomato, ppk-CD4-tdGFP,* or *ppk-Gal4,UAS-CD4-tdGFP* (Han et al., 2011), C1da neurons using *nompC-Gal4, UAS-CD4-tdTo-mato*, C3 da neurons using *19–12-Gal4, UAS-CD4-tdGFP*. For comparison, abdominal segments A3 and A4 were chosen. Confocal stacks were taken with a 20x objective (Zeiss, NA 0.8) to image the whole dendritic field of ddaC neurons. For higher resolution and magnification a 40x oil objective was used (Zeiss, NA 1.3). The chosen z-step size varied from 0.3 – 0.7μm depending on the experiment.

For analysis of dendrite turnover, C4da neurons (ddaC) in abdominal segments A3 or A4 were imaged at 72h AEL and again 24h later (96h AEL). The imaged larvae were allowed to develop to adulthood to ensure that handling and imaging did not interfere with normal development.

Imaging of dendrite-ECM interaction was performed as described using *troll-GFP;ppkCD4-tdTomato* (Soba et al., 2015). Two-color high resolution confocal stacks of the dorsal field of C4da neurons (ddaC) in 3rd instar larvae (96h AEL) were taken using a high NA oil objective (Zeiss 40×, NA 1.3) with a step size of 300 nm.

Immunohistochemistry—Larval filet preparation and immunostaining was performed as described with some modifications (Soba et al., 2015). The following antibodies were used: guinea-pig anti-Ret (kindly provided by I. Miguel-Aliaga), rabbit anti-GFP (A11122, ThermoFisher), mouse anti-coracle (DSHB, Iowa), rat anti-HA (3F10, Roche). Corresponding dye-coupled secondary and Alexa647-coupled anti-horseradish peroxidase (HRP) antibodies were used (Jackson ImmunoResearch, Westgrove, PA).

3rd instar larvae fillets were prepared in Ringer solution. The animals were cut open ventrally after pinning the anterior and the pos-terior ends using insect pins (FST, Heidelberg). The interior organs and fat bodies were removed and the body wall was then flattened with additional pins. Fillets were washed with Ringer solution and fixed with 4% Formaldehyde/PBS for 15 min. After fixation the larval fillets were washed with 0.3% Triton X-100 in PBS (PBS-T) and blocked for 1 h at room temperature (RT) in 5% normal donkey serum (Jackson ImmunoResearch). The samples were incubated with the primary antibody over night at 4° C in 5% donkey serum/PBS, while the secondary antibody was applied at RT for 1 h. After primary and secondary antibody incubation the fillets were washed with PBS-T 3×5min to remove residual antibody solution. After the immunostaining procedure, the samples were transferred to an equilibration buffer (Slowfade Gold, ThermoFisher) and mounted on a glass slide with the muscle side facing down. Silicon was applied on the slide to serve as a spacer and fillets were covered with a coverslip by carefully pressing it down. The mounting medium (Slowfade Gold/50% glycerol in PBS, ThermoFisher) was applied to the sample between the slide and the coverslip. A lead weight was used to flatten the samples and coverslips were then sealed with nail polish. Images were taken on a Zeiss LSM700 confocal microscope with a 20×/0.8NA air lens or with a 40×/1.3NA oil lens.

For immunostaining under non-permeabilizing conditions, Triton X-100 was omitted during all steps and PBS was used instead.

FACS sorting of C4da neurons and microarray hybridization—Microarray analysis was performed using previously described procedures (Jiang et al., 2014) with minor modifications. Body wall filets of 3rd instar larvae were dissociated to single cell suspensions in PBS containing 1 mg/ml collagenase for 20min at 37° C with automated mixing at 1000 rpm (Eppendorf Thermomixer). Samples were triturated 10× through a P1000 pipette tip every 5min during the incubation. C4da neurons were isolated by flow cytometry into 300μl PBS using a FACSAria (BD Biosciences), and immediately re-sorted into 100μl RNAqueous Micro Lysis buffer (ThermoFisher). Samples were flick-mixed and immediately frozen on dry ice. RNA was isolated using the RNAqueous Micro kit (ThermoFisher) as per the manufacturer's protocol, and RNA was amplified using two rounds of linear amplification using the Aminoallyl MessageAmp II kit (Life Technologies). Dye-coupled aRNA was fragmented and hybridized to custom-designed 8×60k gene expression microarrays as per the manufacturer recommen-dations (Agilent Technologies). The microarray design used in this study was previously described (Lin et al., 2015), and details of the platform are available in the NCBI Gene Expression Omnibus under Accession number GPL19582.

QUANTIFICATION AND STATISTICAL ANALYSIS

Dendrite analysis—Dendrites of da neurons were traced semi-automatically using the Imaris Filament Tracer module (BitPlane AG, Zürich,Switzerland). Total dendritic length, branch number and Strahler analysis was calculated from the generated filaments using Imaris. Dendritic crossing points were counted and manually confirmed as non-contacting by visual inspection of the z stack.

Dendritic field coverage was calculated by measuring the area covered by dendrites divided by the total area of the segment (Fiji, ImageJ, NIH).

Dendrite growth/retraction analysis at 72 and 96h AEL was performed as previously described (Soba et al., 2015). Confocal Z-projections of the same neuron at 72 and 96 h AEL were overlayed as 2 channels in ImageJ and adjusted for position and interstitial growth with bUnwarpJ (Fiji, ImageJ, NIH). Landmarks marking all major branch points were used to get accurate overlay images. Growing (branch is shorter at 72 h than 96 h AEL) and retracting (branch is longer at 72 h than 96 h AEL) portions of dendrites were traced using Imaris Filament Tracer (BitPlane) and growth/retraction values were normalized to the total length of the un-changed portion of the dendritic tree at 96 h AEL. Statistical significance was calculated using a Mann-Whitney U-test (Origin Pro).

The analysis of dendrite-ECM interaction was performed as described (Soba et al., 2015). After blind deconvolution (AutoQuant, Bitplane), a colocalization analysis of C4da neuron dendrites and the ECM was performed. Non-contacting and contacting dendrites were semi-automatically traced and verified manually. Percentages of detached dendrites were calculated by the ratios of detached to total dendrites. Statistical significance was analyzed using the non-parametric Mann-Whitney U-Test (Origin Pro).

Analysis of dendrite growth preference and local dendrite coverage—For local manipulations of Mav levels, dendritic filament length in a 100μm wide segment of the anterior/posterior (*en-Gal4*) or dorsal/ventral (*ush-Gal4*) field of C4da neurons was quantified using Imaris Filament Tracer (Bitplane).

Low and high frequency mosaic expression of UAS-mav or mav-RNAi in epithelial cells was achieved using epithelial specific Flip lines (Poe et al., 2017) together with actin > FRT > y^+ > FRT > Gal4. Epithelial Gal4 expression was visualized by UAS-CD8-GFP and C4da neurons using *ppk-CD4-tdTomato* in 3rd instar larvae. For low frequency mosaics, the effect of Mav overexpression or RNAi on local dendrite coverage was analyzed by quantifying dendrite length of C4da neurons covering individual epithelial cells (Imaris Filament Tracer, Bitplane). For high frequency mosaics, C4da neuron dendrite length in equally sized GFP-negative and -positive areas was compared. To address non-autonomous effects of Mav manipulation, an equally sized region surrounding positively GFP-labeled epithelial cells was drawn (red areas) and dendrite length covering this area was quantified. All data were normalized to the analyzed area.

Heat-maps and assessment of dendrite distribution—Heat-maps were generated to create a visual representation using Fiji (ImageJ) on the basis of dendritic filaments of

individual cells. The dendritic width of these filaments was reduced to one pixel, thus taking each dendritic section equally into account. Neurons were then matched in their orientation (dorsal/ventral; anterior/posterior) and aligned at the soma. Subsequently, filaments were projected onto each other followed by the application of a mean filter (Radius = 50px) to yield a probabilistic distribution. To put an emphasis on areas with a higher occurrence of dendritic material an RGB-LUT was applied with the intensity values adjusted to exploit the full color scale.

For quantitative assessment of the dendritic coverage within the dendritic field, coordinates of non-background pixels were ex-tracted from images of the dendritic filament and evaluated regarding their angular and radial position. Therefore, the centroid of the soma was used as a reference as well as a vector pointing vertically upward from aforementioned point. Applying formula (1) the angular distribution was assessed, correcting for angles > 180 . These values were then divided into 40 bins (340° −20°; 20° −60°, etc.) as well as into sub bins according to their radial distribution in respect of their range from the center within the dendritic field (33%, 66%, 100%). These data were then depicted as average percentages per cell in a customized rose plot generated with Excel (Microsoft Corp.).

$$\cos(\alpha) = \frac{\vec{a} * \vec{b}}{\left|\vec{a}\right| * \left|\vec{b}\right|}, 0° < \alpha < 180° \quad \text{(Equation 1)}$$

Quantitative immunohistochemical analysis—For quantitative analysis of anti-Ret immunofluorescence signals, the soma region of C4da neurons in control and Ret^{ko} animals was analyzed in confocal image stacks and signal over background ratios were calculated by subtracting background signal flanking the C4da soma region. Statistical significance of intensity differences was calculated using a Mann-Whitney U-test.

For analysis of Mav-GFP levels in $mav\text{-}GFP^{Fos}$ animals, larval filet preparations were immunostained with anti-GFP, anti-coracle and anti-HRP-Alexa647. Mav-GFP intensity values of individual analyzed epithelial cells were calculated using maximum projections of confocal image stacks of identical thickness (Fiji, ImageJ, NIH).

For analysis of Mav distribution, larval filet preparations of UAS-2xHA-Mav expressing animals (en-Gal4 or LF-Flp) were immuno-stained using a rat anti-HA antibody (1:300) with or without 0.3% Triton X-100 (TX-100) to visualize total or surface Mav levels, respectively. High resolution confocal image stacks were taken and the same body wall region within the dorsal dendritic field of each C4da neuron (ddaC) was analyzed. A 31 μm wide XY section (approx. one row of epithelial cells) was maximally projected in XZ–direction and the Mav signal along the basal epithelial surface was analyzed using a line-ROI (8pt) stretching from the anterior to the anterior part of the segment (ImageJ, NIH). The en-Gal4 expression domain was determined using the corresponding intensity profile of NLS-mCherry expression and aligned for all images to allow quantitative comparison of Mav levels along the anterior-posterior axis within and outside of the expression domain.

Microarray analysis—Microarrays were scanned on an Agilent scanner at 3μm resolution as a 20-bit image, and probe intensities were extracted using Agilent Feature Extraction. Raw Cy3 intensities were extracted and quantile normalized using Limma (Smith, 2005). Differentially expressed genes were identified using Significance Analysis for Microarrays (Tusher et al., 2001). Pairwise comparisons were performed with a false discovery rate of 1% and 2-fold change threshold. Hierarchical clustering and heatmap visualization were performed as previously described (Kim et al., 2012a). Microarray data are available at the NCBI Gene Expression Omnibus (GEO: GSE115500).

QUANTIFICATION AND STATISTICAL ANALYSIS

Statistical analysis was performed using Origin Pro software (OriginLabs). Statistical methods applied to the specific dataset are mentioned in the figure legends. Unless otherwise noted, analyzed data were represented as box-plots with whiskers, with the centerline representing median values, upper, and lower edges of the boxes representing the 25^{th} and 75^{th} percentiles of the sample data, respectively. The small square within the box represents the mean of the data. Upper and lower whiskers represent the 5^{th} and 95^{th} percentile of the sample data, respectively. All data points were additionally shown as diamond-shaped squares. Data were analyzed using a One-way ANOVA with a Bonferroni post hoc test for multiple comparisons unless otherwise noted. Comparison of 2 groups was conducted using a Student's t test or, if normality was not given, was analyzed using the nonparametric Mann-Whitney U-test. For bar graphs, bar height indicates mean value and error bars standard deviations (SD). In all figures, n.s., *, **, and *** represent $p > 0.05$, $p < 0.05$, $p < 0.01$, and $p < 0.001$, respectively.

Supplementary Material

Refer to Web version on PubMed Central for supplementary material.

ACKNOWLEDGMENTS

Stocks obtained from the Bloomington (supported by National Institutes of Health [NIH, United States] grant P40OD018537), Vienna (VDRC), and Kyoto *Drosophila* Stock Centers (DGRC) and antibodies obtained from the Developmental Studies Hybridoma Bank (DSHB) were used in this study. We would like to thank V. Budnik, T. Haerry, and M. O'Connor for fly stocks and reagents; M. Kreutz for critical reading of the original manuscript; D. Clausen for artwork; T. Kidd for communicating results prior to publication. This work was sup-ported by National Institutes of Health (NIH, United States) grants (R01NS099125 and R21OD023824 awarded to C.Han, R01-NS076614 awarded to J.Z.P.), the Landesforschungsfo¨rderung Hamburg (LFF, Germany, LFF-FV27 awarded to. P.S.), and the Deutsche Forschungsgemeinschaft (DFG, Germany) grants (SO1337/2–1 and SO1337/4–1 awarded to P.S.).

REFERENCES

Abrescia C, Sjöstrand D, Kjaer S, and Ibáñez CF (2005). Drosophila RET contains an active tyrosine kinase and elicits neurotrophic activities in mammalian cells. FEBS Lett 579, 3789–3796. [PubMed: 15978587]

Bonanomi D, Chivatakarn O, Bai G, Abdesselem H, Lettieri K, Marquardt T, Pierchala BA, and Pfaff SL (2012). Ret is a multifunctional cor-eceptor that integrates diffusible- and contact-axon guidance signals. Cell 148, 568–582. [PubMed: 22304922]

Brantley MA, Jr., Jain S, Barr EE, Johnson EM, Jr., and Milbrandt J (2008). Neurturin-mediated ret activation is required for retinal function. J. Neurosci 28, 4123–4135. [PubMed: 18417692]

Charalambous P, Wang X, Thanos S, Schober A, and Unsicker K (2013). Regulation and effects of GDF-15 in the retina following optic nerve crush. Cell Tissue Res 353, 1–8. [PubMed: 23640134]

Dong X, Liu OW, Howell AS, and Shen K (2013). An extracellular adhesion molecule complex patterns dendritic branching and morphogenesis. Cell 155, 296–307. [PubMed: 24120131]

Dong X, Shen K, and Bülow HE (2015). Intrinsic and Extrinsic Mechanisms of Dendritic Morphogenesis. Annu. Rev. Physiol 77, 271–300. [PubMed: 25386991]

Emmerson PJ, Wang F, Du Y, Liu Q, Pickard RT, Gonciarz MD, Cos-kun T, Hamang MJ, Sindelar DK, Ballman KK, et al. (2017). The metabolic effects of GDF15 are mediated by the orphan receptor GFRAL. Nat. Med 23, 1215–1219. [PubMed: 28846098]

Esposito CL, D'Alessio A, de Franciscis V, and Cerchia L (2008). A cross-talk between TrkB and Ret tyrosine kinases receptors mediates neuroblastoma cells differentiation. PLoS ONE 3, e1643. [PubMed: 18286198]

Fuentes-Medel Y, Ashley J, Barria R, Maloney R, Freeman M, and Budnik V (2012). Integration of a retrograde signal during synapse formation by glia-secreted TGF-β ligand. Curr. Biol 22, 1831–1838. [PubMed: 22959350]

Gallegos ME, and Bargmann CI (2004). Mechanosensory neurite termination and tiling depend on SAX-2 and the SAX-1 kinase. Neuron 44, 239–249. [PubMed: 15473964]

Gao F-B, Kohwi M, Brenman JE, Jan LY, and Jan YN (2000). Control of dendritic field formation in Drosophila: the roles of flamingo and competition between homologous neurons. Neuron 28, 91–101. [PubMed: 11086986]

Gratz SJ, Cummings AM, Nguyen JN, Hamm DC, Donohue LK, Harrison MM, Wildonger J, and O'Connor-Giles KM (2013). Genome engineering of Drosophila with the CRISPR RNA-guided Cas9 nuclease. Genetics 194, 1029–1035. [PubMed: 23709638]

Groth AC, Fish M, Nusse R, and Calos MP (2004). Construction of transgenic Drosophila by using the site-specific integrase from phage phiC31. Genetics 166, 1775–1782. [PubMed: 15126397]

Grueber WB, Jan LY, and Jan YN (2002). Tiling of the Drosophila epidermis by multidendritic sensory neurons. Development 129, 2867–2878. [PubMed: 12050135]

Hahn M, and Bishop J (2001). Expression pattern of Drosophila ret suggests a common ancestral origin between the metamorphosis precursors in insect endoderm and the vertebrate enteric neurons. Proc. Natl. Acad. Sci. USA 98, 1053–1058. [PubMed: 11158593]

Hakeda S, and Suzuki T (2013). Golden goal controls dendrite elongation and branching of multidendritic arborization neurons in Drosophila. Genes Cells 18, 960–973. [PubMed: 23919529]

Han C, Jan LY, and Jan Y-NN (2011). Enhancer-driven membrane markers for analysis of nonautonomous mechanisms reveal neuron-glia interactions in Drosophila. Proc. Natl. Acad. Sci. USA 108, 9673–9678. [PubMed: 21606367]

Han C, Wang D, Soba P, Zhu S, Lin X, Jan LY, and Jan Y-N (2012). Integrins regulate repulsion-mediated dendritic patterning of Drosophila sensory neurons by restricting dendrites in a 2D space. Neuron 73, 64–78. [PubMed: 22243747]

Hattori Y, Usui T, Satoh D, Moriyama S, Shimono K, Itoh T, Shirahige K, and Uemura T (2013). Sensory-neuron subtype-specific transcriptional programs controlling dendrite morphogenesis: genome-wide analysis of Abrupt and Knot/Collier. Dev. Cell 27, 530–544. [PubMed: 24290980]

Hernández K, Myers LG, Bowser M, and Kidd T (2015). Genetic Tools for the Analysis of Drosophila Stomatogastric Nervous System Development. PLoS ONE 10, e0128290. [PubMed: 26053861]

Hsu J-Y, Crawley S, Chen M, Ayupova DA, Lindhout DA, Higbee J, Kutach A, Joo W, Gao Z, Fu D, et al. (2017). Non-homeostatic body weight regulation through a brainstem-restricted receptor for GDF15. Nature 550, 255–259. [PubMed: 28953886]

Huang J, Zhou W, Dong W, Watson AM, and Hong Y (2009). From the Cover: Directed, efficient, and versatile modifications of the Drosophila genome by genomic engineering. Proc. Natl. Acad. Sci. USA 106, 8284–8289. [PubMed: 19429710]

Hughes ME, Bortnick R, Tsubouchi A, Bäumer P, Kondo M, Uemura T, and Schmucker D (2007). Homophilic Dscam interactions control complex dendrite morphogenesis. Neuron 54, 417–427. [PubMed: 17481395]

Ibáñez CF (2013). Structure and physiology of the RET receptor tyrosine kinase. Cold Spring Harb. Perspect. Biol 5, a009134. [PubMed: 23378586]

Jiang N, Soba P, Parker E, Kim CC, and Parrish JZ (2014). The micro-RNA bantam regulates a developmental transition in epithelial cells that restricts sensory dendrite growth. Development 141, 2657–2668. [PubMed: 24924190]

Kallijärvi J, Stratoulias V, Virtanen K, Hietakangas V, Heino TI, and Saarma M (2012). Characterization of Drosophila GDNF receptor-like and evidence for its evolutionarily conserved interaction with neural cell adhesion molecule (NCAM)/FasII. PLoS ONE 7, e51997. [PubMed: 23284846]

Kim NC, and Marqués G (2010). Identification of downstream targets of the bone morphogenetic protein pathway in the Drosophila nervous system. Dev. Dyn 239, 2413–2425. [PubMed: 20652954]

Kim CC, Nelson CS, Wilson EB, Hou B, DeFranco AL, and DeRisi JL (2012a). Splenic red pulp macrophages produce type I interferons as early sentinels of malaria infection but are dispensable for control. PLoS ONE 7, e48126. [PubMed: 23144737]

Kim ME, Shrestha BR, Blazeski R, Mason CA, and Grueber WB (2012b). Integrins establish dendrite-substrate relationships that promote dendritic self-avoidance and patterning in Drosophila sensory neurons. Neuron 73, 79–91. [PubMed: 22243748]

Kramer ER, Knott L, Su F, Dessaud E, Krull CE, Helmbacher F, and Klein R (2006). Cooperation between GDNF/Ret and ephrinA/EphA4 signals for motor-axon pathway selection in the limb. Neuron 50, 35–47. [PubMed: 16600854]

Lefebvre JL, Kostadinov D, Chen WV, Maniatis T, and Sanes JR (2012). Protocadherins mediate dendritic self-avoidance in the mammalian nervous system. Nature 488, 517–521. [PubMed: 22842903]

Lefebvre JL, Sanes JR, and Kay JN (2015). Development of dendritic form and function. Annu. Rev. Cell Dev. Biol 31, 741–777. [PubMed: 26422333]

Lin WY, Williams C, Yan C, Koledachkina T, Luedke K, Dalton J, Bloomsburg S, Morrison N, Duncan KE, Kim CC, and Parrish JZ (2015). The SLC36 transporter Pathetic is required for extreme dendrite growth in Drosophila sensory neurons. Genes Dev 29, 1120–1135. [PubMed: 26063572]

Liu OW, and Shen K (2011). The transmembrane LRR protein DMA-1 promotes dendrite branching and growth in C. elegans. Nat. Neurosci 15, 57–63. [PubMed: 22138642]

Matsubara D, Horiuchi S-Y, Shimono K, Usui T, and Uemura T (2011). The seven-pass transmembrane cadherin Flamingo controls dendritic self-avoidance via its binding to a LIM domain protein, Espinas, in Drosophila sensory neurons. Genes Dev 25, 1982–1996. [PubMed: 21937715]

Matthews BJ, Kim ME, Flanagan JJ, Hattori D, Clemens JC, Zipursky SL, and Grueber WB (2007). Dendrite self-avoidance is controlled by Dscam. Cell 129, 593–604. [PubMed: 17482551]

Meltzer S, Yadav S, Lee J, Soba P, Younger SH, Jin P, Zhang W, Parrish J, Jan LY, and Jan Y-N (2016). Epidermis-Derived Semaphorin Promotes Dendrite Self-Avoidance by Regulating Dendrite-Substrate Adhesion in Drosophila Sensory Neurons. Neuron 89, 741–755. [PubMed: 26853303]

Mullican SE, Lin-Schmidt X, Chin CN, Chavez JA, Furman JL, Armstrong AA, Beck SC, South VJ, Dinh TQ, Cash-Mason TD, et al. (2017). GFRAL is the receptor for GDF15 and the ligand promotes weight loss in mice and nonhuman primates. Nat. Med 23, 1150–1157. [PubMed: 28846097]

Myers L, Perera H, Alvarado MG, and Kidd T (2018). The Drosophila Ret gene functions in the stomatogastric nervous system with the Maverick TGFβ ligand and the Gfrl co-receptor. Development 145, dev157446.

Nguyen M, Parker L, and Arora K (2000). Identification of maverick, a novel member of the TGF-beta superfamily in Drosophila. Mech. Dev 95, 201–206. [PubMed: 10906462]

Perea D, Guiu J, Hudry B, Konstantinidou C, Milona A, Hadjieconomou D, Carroll T, Hoyer N, Natarajan D, Kallijärvi J, et al. (2017). Ret receptor tyrosine kinase sustains proliferation and tissue maturation in intestinal epithelia. EMBO J 36, 3029–3045. [PubMed: 28899900]

Peterson AJ, and O'Connor MB (2014). Strategies for exploring TGF-β signaling in Drosophila. Methods 68, 183–193. [PubMed: 24680699]

Poe AR, Tang L, Wang B, Li Y, Sapar ML, and Han C (2017). Dendritic space-filling requires a neuronal type-specific extracellular permissive signal in Drosophila. Proc. Natl. Acad. Sci. USA 114, E8062–E8071. [PubMed: 28874572]

Port F, Chen H-M, Lee T, and Bullock SL (2014). Optimized CRISPR/Cas tools for efficient germline and somatic genome engineering in Drosophila. Proc. Natl. Acad. Sci. USA 111, E2967–E2976. [PubMed: 25002478]

Saarma M (2000). GDNF - a stranger in the TGF-β superfamily? Eur. J. Biochem 267, 6968–6971. [PubMed: 11106404]

Sagasti A, Guido MR, Raible DW, and Schier AF (2005). Repulsive interactions shape the morphologies and functional arrangement of zebrafish peripheral sensory arbors. Curr. Biol 15, 804–814. [PubMed: 15886097]

Salzberg Y, Díaz-Balzac CA, Ramirez-Suarez NJ, Attreed M, Tecle E, Desbois M, Kaprielian Z, and Bulow HE (2013). Skin-derived cues control arborization of sensory dendrites in Caenorhabditis elegans. Cell 155, 308–320. [PubMed: 24120132]

Sarov M, Barz C, Jambor H, Hein MY, Schmied C, Suchold D, Stender B, Janosch S, K J V, Krishnan RT, et al. (2016). A genome-wide resource for the analysis of protein localisation in Drosophila. eLife 5, e12068. [PubMed: 26896675]

Smith GK (2005). Limma: linear models for microarray data. In Bioinformatics and Computational Biology Solutions Using R and Bioconductor, Gentleman R, Carey V, Dudoit S, Irizarry R, and Huber W, eds. (New York: Springer), pp. 397–420.

Soba P, Zhu S, Emoto K, Younger S, Yang S-J, Yu H-H, Lee T, Jan LY, and Jan Y-N (2007). Drosophila sensory neurons require Dscam for dendritic self-avoidance and proper dendritic field organization. Neuron 54, 403–416. [PubMed: 17481394]

Soba P, Han C, Zheng Y, Perea D, Miguel-Aliaga I, Jan LY, and Jan YN (2015). The Ret receptor regulates sensory neuron dendrite growth and integrin mediated adhesion. eLife 4, e05491.

Sugaya R, Ishimaru S, Hosoya T, Saigo K, and Emori Y (1994). A Drosophila homolog of human proto-oncogene ret transiently expressed in embryonic neuronal precursor cells including neuroblasts and CNS cells. Mech. Dev 45, 139–145. [PubMed: 8199050]

Sun LO, Jiang Z, Rivlin-Etzion M, Hand R, Brady CM, Matsuoka RL, Yau K-W, Feller MB, and Kolodkin AL (2013). On and off retinal circuit assembly by divergent molecular mechanisms. Science 342, 1241974. [PubMed: 24179230]

Ting C-Y, McQueen PG, Pandya N, Lin T-Y, Yang M, Reddy OV, O'Connor MB, McAuliffe M, and Lee C-H (2014). Photoreceptor-derived activin promotes dendritic termination and restricts the receptive fields of first-order interneurons in Drosophila. Neuron 81, 830–846. [PubMed: 24462039]

Tufro A, Teichman J, Banu N, and Villegas G (2007). Crosstalk between VEGF-A/VEGFR2 and GDNF/RET signaling pathways. Biochem. Biophys. Res. Commun 358, 410–416. [PubMed: 17490619]

Tusher VG, Tibshirani R, and Chu G (2001). Significance analysis of microarrays applied to the ionizing radiation response. Proc. Natl. Acad. Sci. USA 98, 5116–5121. [PubMed: 11309499]

Venken KJT, Schulze KL, Haelterman NA, Pan H, He Y, Evans-Holm M, Carlson JW, Levis RW, Spradling AC, Hoskins RA, and Bellen HJ (2011). MiMIC: a highly versatile transposon insertion resource for engineering Drosophila melanogaster genes. Nat. Methods 8, 737–743. [PubMed: 21985007]

Wang Z, and Mann RS (2003). Requirement for two nearly identical TGIF-related homeobox genes in Drosophila spermatogenesis. Development 130, 2853–2865. [PubMed: 12756170]

Wässle H, and Boycott BB (1991). Functional architecture of the mammalian retina. Physiol. Rev 71, 447–480. [PubMed: 2006220]

Yan D, and Lin X (2009). Shaping morphogen gradients by proteoglycans. Cold Spring Harb. Perspect. Biol 1, a002493. [PubMed: 20066107]

Yan Z, Zhang W, He Y, Gorczyca D, Xiang Y, Cheng LE, Meltzer S, Jan LY, and Jan YN (2013). Drosophila NOMPC is a mechanotransduction channel subunit for gentle-touch sensation. Nature 493, 221–225. [PubMed: 23222543]

Yang L, Chang C-C, Sun Z, Madsen D, Zhu H, Padkjær SB, Wu X, Huang T, Hultman K, Paulsen SJ, et al. (2017). GFRAL is the receptor for GDF15 and is required for the anti-obesity effects of the ligand. Nat. Med 23, 1158–1166. [PubMed: 28846099]

Zhang J, Ma W, Tian S, Fan Z, Ma X, Yang X, Zhao Q, Tan K, Chen H, Chen D, and Huang BR (2014). RanBPM interacts with TbRI, TRAF6 and curbs TGF induced nuclear accumulation of TbRI. Cell. Signal 26, 162–172. [PubMed: 24103590]

Zipursky SL, and Grueber WB (2013). The molecular basis of self-avoidance. Annu. Rev. Neurosci 36, 547–568. [PubMed: 23841842]

Highlights

- Substrate-derived TGF-β Maverick is required for dendrite patterning of C4da neurons
- Maverick acts upstream of the neuronal Ret receptor
- Local extracellular Maverick levels are regulated by *Ret*-dependent neuronal uptake
- Growth is directed toward higher Maverick levels to ensure dendrite space-filling

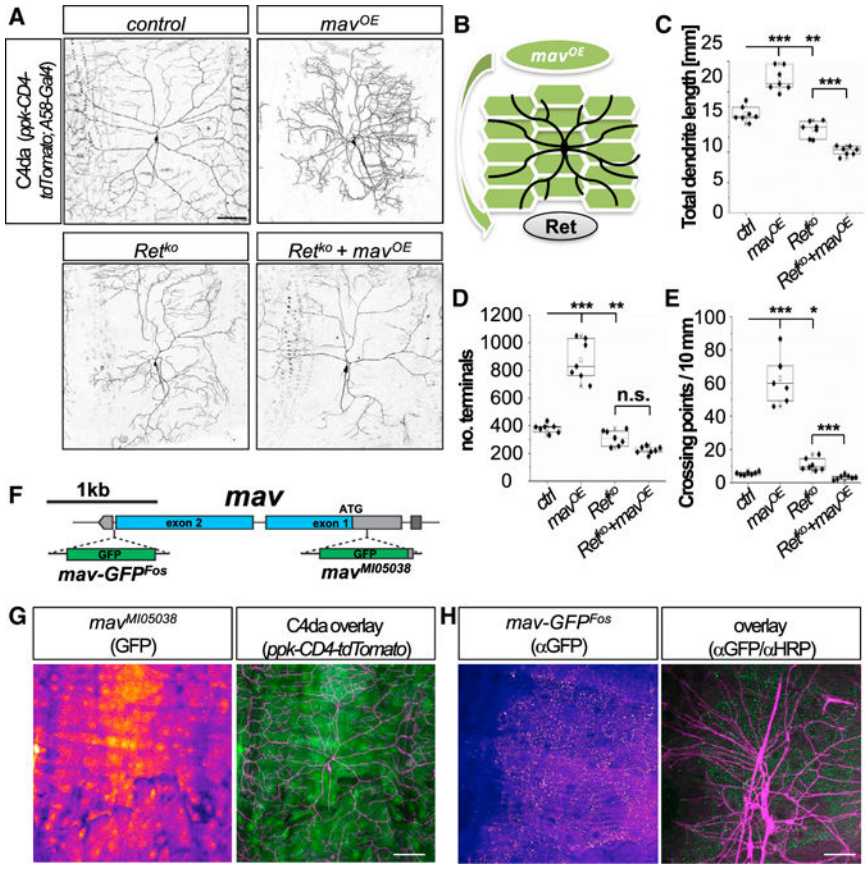

Figure 1. Epithelial Mav Expression Affects C4da Neuron Dendrite Patterning in a *Ret*-Dependent Manner

(A) C4da neurons (*ppk-CD4-tdTomato*) in control and Ret^{ko} third-instar larvae with or without epithelial overexpression of Mav using *A58-Gal4*. Scale bar, 100 μm.

(B) Schematic illustration of Ret-expressing C4da neurons and epithelial cells overexpressing Mav (mav^{OE}) as shown in (A).

(C–E) Quantitative analysis of (C) total dendrite length, (D) number of terminals, and (E) isoneuronal dendritic crossing of C4da neuron dendrites of the indicated genotypes. n = 7/genotype, one-way ANOVA, Bonferroni post hoc test, *p < 0.05, **p < 0.01, ***p < 0.001. Center lines of boxes represent median values; small squares are average values; upper and lower edges of the boxes represent the 75th and 25th percentiles of the sample data, respectively; whiskers represent 95th and 5th percentiles of the sample data.

(F) Schematic *mav* locus consisting of 3 exons (coding region in blue, untranslated regions in gray). The insertion site of a GFP enhancer reporter ($mav^{MI05038}$) and a fosmid transgene containing the GFP-tagged genomic *mav* locus ($mav\text{-}GFP^{Fos}$) are shown.

(G) GFP expression of $mav^{MI05038}$ in third-instar larvae (96 hr AEL, *ppk-CD4-tdTomato*) in the larval body wall epithelium. Scale bar, 100 μm.

(H) Mav-GFP expression in $mav\text{-}GFP^{Fos}$ thirdinstar larvae (96 hr AEL) visualized by anti-GFP and anti-HRP (sensory neuron marker) immunostaining. Mav-GFP puncta were visible in epithelial cells of the entire body wall overlapping with sensory neuron receptive fields. Scale bar, 50 μm.

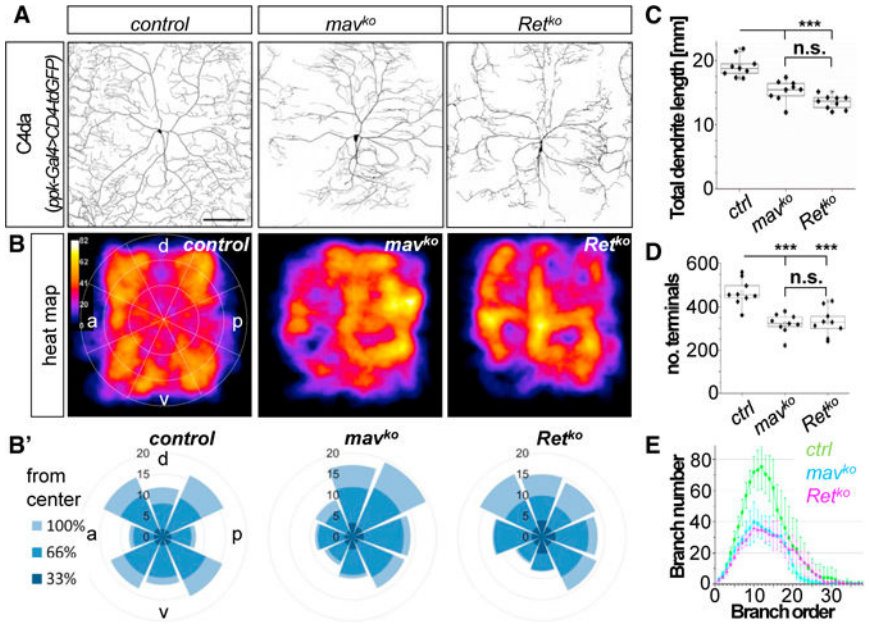

Figure 2. *Mav* and *Ret* Loss of Function Equally Impair Radial Dendrite Growth and Complexity of C4da Neurons

(A) Dendritic morphology of C4da neurons in control, mav^{ko}, and Ret^{ko} third-instar larvae (*ppk-Gal4,UAS-CD4-tdGFP*). Scale bar, 100 μm.

(B) Qualitative heatmaps showing cumulative distribution of C4da neuron dendrites (n = 5, 5, 6; a, anterior; p, posterior; d, dorsal; v, ventral). (B') Quantitative rose plot analysis of C4da neuron dendrite distribution within proximal, medial, and distal field areas representing the 33, 66, and 100 field percentile, respectively (illustrated in B; n = 5, 5, 6).

(C–E) Quantitative analysis of (C) total dendrite length, (D) terminal numbers, and (E) dendrite complexity by Strahler analysis in control, mav^{ko}, and Ret^{ko} third-instar larvae (n = 9, mean ± SD, one-way ANOVA, Bonferroni post hoc test, ***p < 0.001).

Center lines of boxes represent median values; small squares are average values; upper and lower edges of the boxes represent the 75th and 25th percentiles of the sample data, respectively; whiskers represent 95th and 5th percentiles of the sample data.

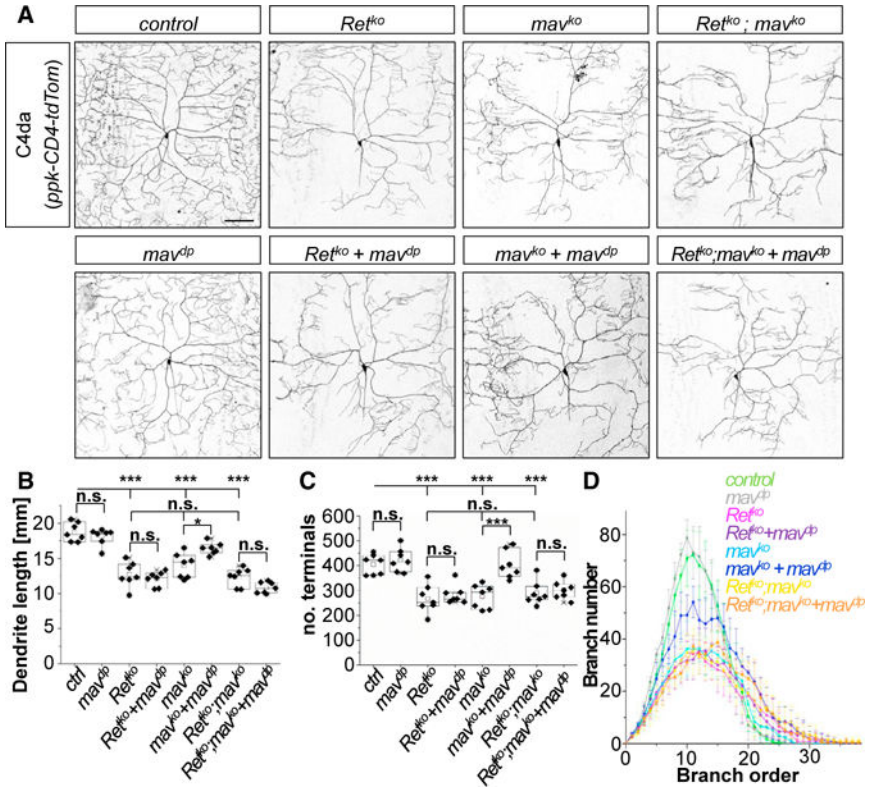

Figure 3. *Mav* Functions Upstream of *Ret* in the Same Genetic Pathway

(A) C4da neurons (*ppk-CD4-tdTomato*) from control, Ret^{ko}, mav^{ko}, and Ret^{ko};mav^{ko} third-instar larvae with and without a genomic *mav* duplication (mav^{dp}). Scale bar, 100 μm.

(B–D) Quantitative analysis of C4da neuron (B) dendrite length, (C) number of terminals, and (D) dendrite complexity by Strahler analysis of indicated genotypes. C4 da neuron dendrite defects in Ret^{ko} and mav^{ko} were not enhanced in double knockout larvae. *Mav* duplication was able to significantly rescue mav^{ko} but not Ret^{ko} or Ret^{ko};mav^{ko} double knockout defects in C4da neurons. n = 7, mean ± SD, one-way ANOVA, Bonferroni post hoc test, ***p < 0.001).

Center lines of boxes represent median values; small squares are average values; upper and lower edges of the boxes represent the 75th and 25th percentiles of the sample data, respectively; whiskers represent 95th and 5th percentiles of the sample data.

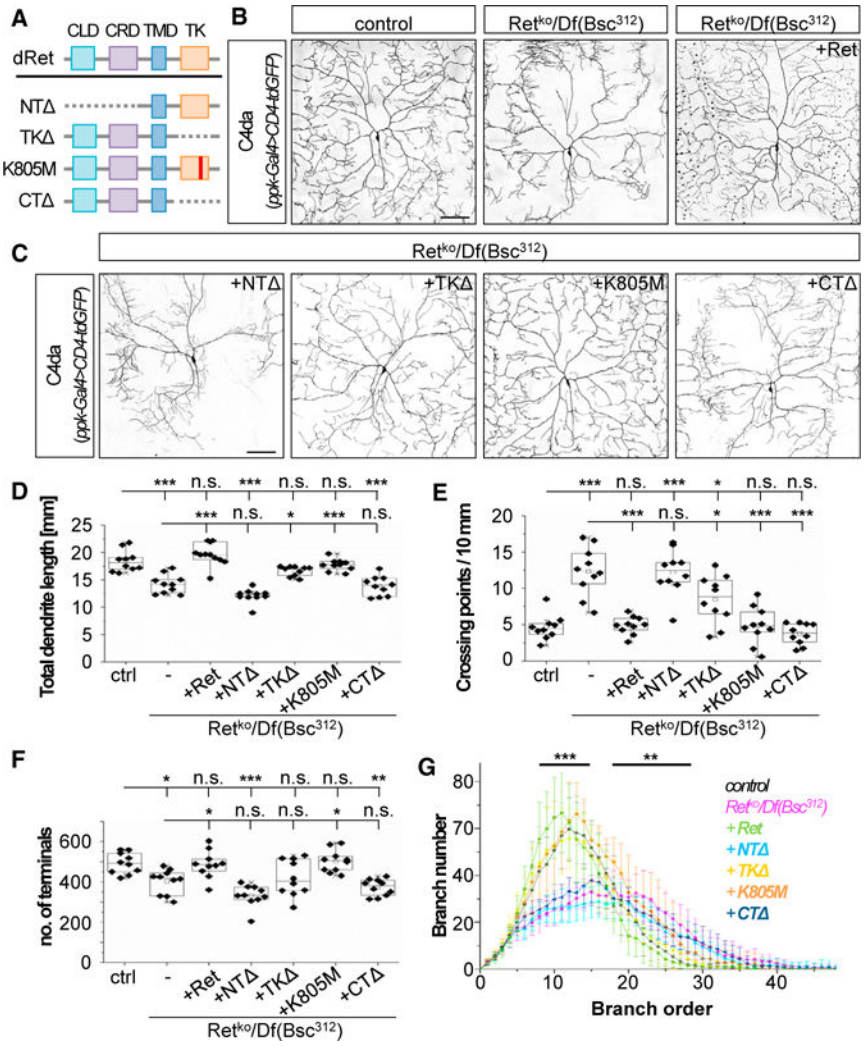

Figure 4. *Ret* Function in C4da Neuron Dendrite Development Requires Its Extraand Intracellular Domains.

(A) Ret protein domain organization and domain deletion transgenes. Ret, full-length Ret protein; NTD, extracellular domain deletion; TKΔ, tyrosine kinase domain deletion; RetK805M, kinase-dead; CTΔ, intracellular domain deletion.

(B and C) C4da neurons in (B) control and Ret^{ko} third-instar larvae with or without C4da neuronspecific *UAS-Ret* expression (*ppk-Gal4, UASCD4-tdGFP*), or (C) with expression of different Ret domain deletions (described in A). Scale bars, 100 μm.

(D–G) Quantitative analysis of C4da neuron (D) total dendrite length, (E) isoneuronal dendritic crossing, (F) terminal numbers, and (G) dendrite complexity assessed by Strahler analysis. Fulllength Ret, Ret-K805M, and TKΔ could significantly rescue all parameters, whereas Ret lacking the entire intra- or extracellular domain showed no rescue activity. n = 10 per genotype, mean ± SD, one-way ANOVA, Bonferroni *post hoc* test, *p < 0.05, **p < 0.01, ***p < 0.001).

Center lines of boxes represent median values; small squares are average values; upper and lower edges of the boxes represent the 75th and 25th percentiles of the sample data, respectively; whiskers represent 95th and 5th percentiles of the sample data.

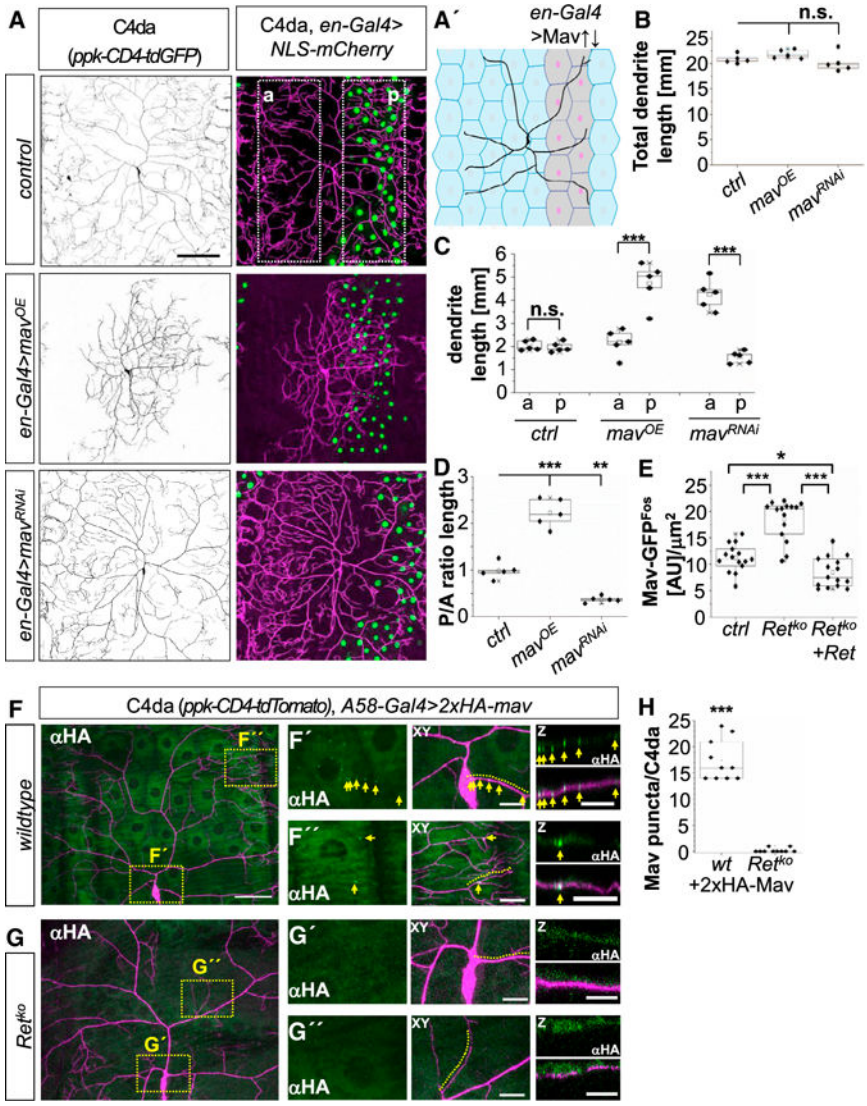

Figure 5. Local Mav Levels Control Dendrite Growth Preference and Are Regulated by *Ret*-Dependent Neuronal Uptake.

(A) Third-instar C4da neurons (*ppk-CD4-tdGFP*) in control animals or with overexpression of Mav (*mav*^{OE}) or Mav-RNAi (*mav*^{RNAi}) in the posterior epithelium (*en-Gal4* > NLS-mCherry; green). Scale bar, 100 µm.

(B–D) Quantitative analysis of C4da neuron dendrite length of the (B) total, (C) anterior (a) and posterior (p) field region (the boxes in A indicate analyzed anterior to posterior compartments) and (D) ratio of dendrite length between posterior and anterior fields (n = 5, one-way ANOVA, Bonferroni *post hoc* test, **p < 0.01, ***p < 0.001).

(E) Quantitative analysis of epithelial Mav-GPF intensity (*ppk-Gal4, UAS-CD4-tdTomato; mav-GFP*^{Fos}) in control and *Ret*^{ko} animals without and with C4da neuron-specific Ret overexpression (n = 15, epithelial cells from n > 3 animals/genotype, one-way ANOVA, Bonferroni *post hoc* test, *p <0.05, ***p < 0.001). In *Ret*^{ko} animals, Mav-GFP levels were strongly increased but reduced by C4da neuron-specific overexpression of Ret.

(F and G) Epithelial overexpression and immunostaining of HA-tagged Mav (*ppk-CD4-tdTomato; A58-Gal4*) in (F) wild-type and (G) Ret^{ko} third-instar larvae. Scale bar, 50 μm. The boxed regions in (F) and (G) indicate enlarged images of the C4da neuron soma region (F' and G') and distal dendrites (F'' and G''). Arrows in XY/Z plane (dendrite sliced along the dotted yellow line) indicate specific Mav puncta (anti-HA) in proximal (F') and distal (F'') C4da neuron dendrites in controls that were absent in Ret^{ko} animals. Scale bars, 15 μm. (H) Quantitative analysis of Mav puncta in C4da neurons in wild-type and Ret^{ko} animals (n = 10/genotype, Mann-Whitney *U* test, ***$p < 0.001$).

Center lines of boxes represent median values; small squares are average values; upper and lower edges of the boxes represent the 75th and 25th percentiles of the sample data, respectively; whiskers represent 95th and 5th percentiles of the sample data.

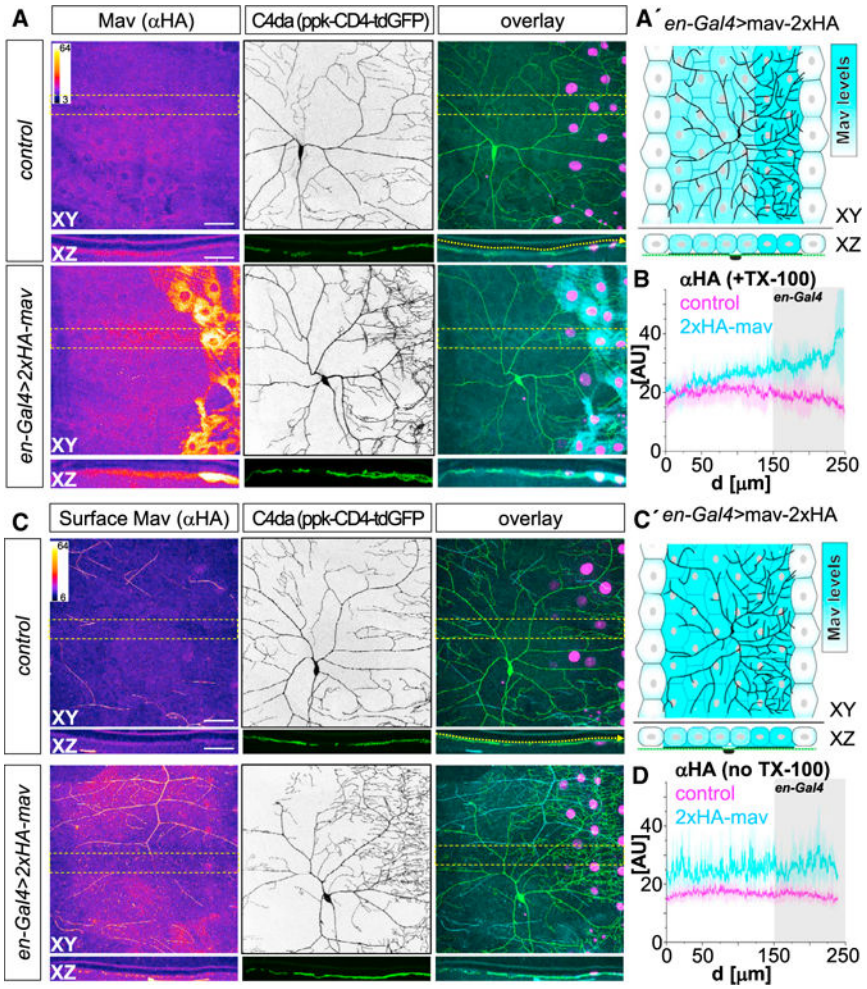

Figure 6. Mav Is Secreted and Can Diffuse across the Body Wall Epithelium.

(A) Immunohistochemical analysis (IHC) of thirdinstar larval filets (*en-Gal4,UAS-NLS-mCherry, ppk-CD4-tdGFP*) under permeabilizing conditions (anti-HA, +Triton X-100 [TX-100]). Nuclear mCherry (in magenta) labels the epithelial expression domain of *en-Gal4* in controls and for overexpression of HA-tagged Mav. XY and partial XZ projections are shown (the boxed region indicates the shown XZ projection). Scale bars, 50 μm. (A') Schematic C4da neuron and epithelium in XY/XZ planes, indicating Mav levels.

(B) Quantitative intensity profiles of the Mav signal within the basal epithelial region lining C4da neuron dendrites along the anterior to posterior axis (indicated by the line in A, +TX-100, n = 3, mean ± SD). The gray area indicates the *en-Gal4* expression domain.

(C) IHC of third-instar larval filets under non-permeabilizing conditions (anti-HA, no TX-100). Note the widespread distribution of Mav along the basal epithelial surface. Scale bars, 50 μm. (C') Schematic distribution of Mav at the basal epithelial surface.

(D) Quantitative intensity profiles of the Mav signal in the basal epithelial region lining C4da neuron dendrites along the anterior to posterior axis (indicated by the dotted line in C, no TX-100, n = 4, mean ± SD).

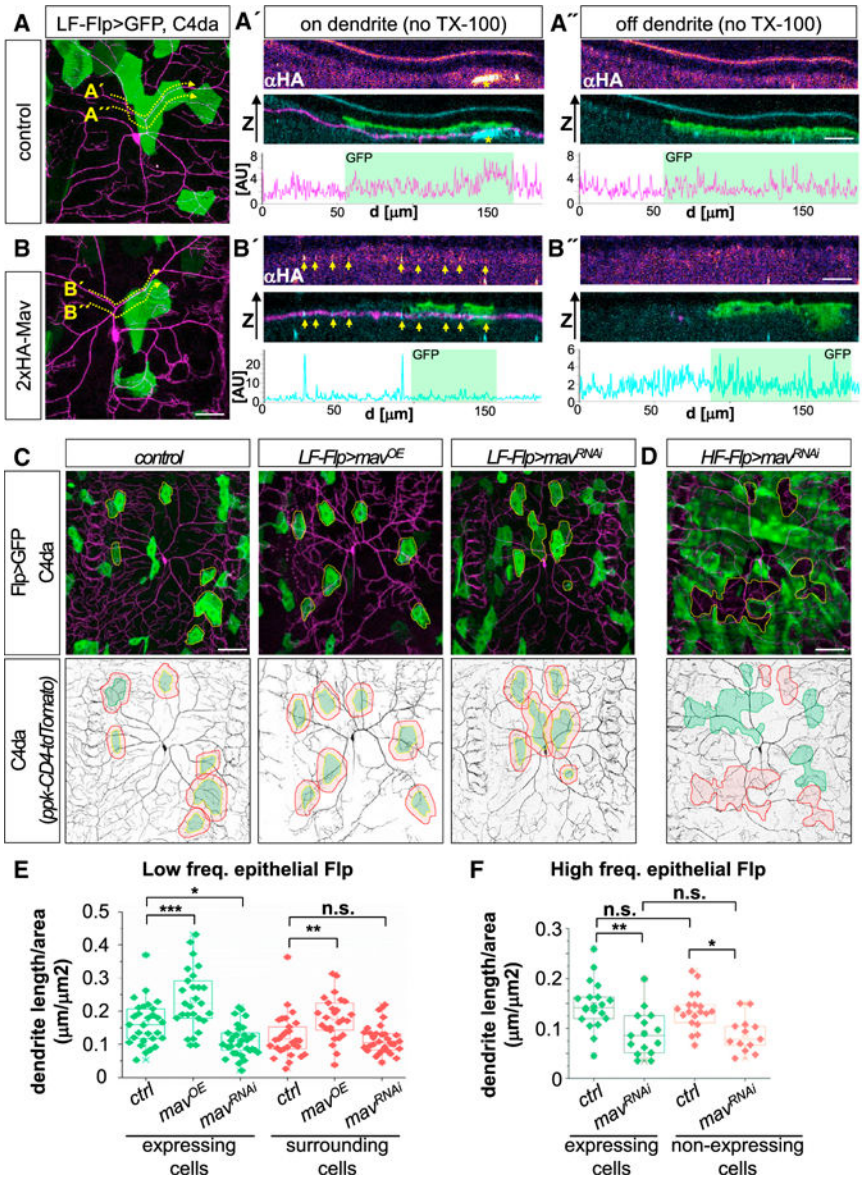

Figure 7. Local and Proximal Control of C4da Neuron Dendrite Growth by Epithelial Mav Levels

(A and B) IHC of third-instar larval filets under nonpermeabilizing conditions (anti-HA, no TX-100). Shown are (A) control or (B) overexpression of HA-tagged Mav in epithelial clones using a lowactivity Flp line (*LF-Flp, actin- > FRT > y+ > FRT > Gal4,UAS-GFP*). XZ projections sliced either along or off dendrites (indicated by lines) are shown for control (A' and A'') and Mav overexpression (B' and B''). Intensity profiles of the extracellular Mav signal along the basal epithelial region lining C4 da neuron dendrites are shown (GFP-expressing epithelial clone in green). The specific Mav signal (indicated by arrows in B'; the asterisks in A' indicate a nonspecific tracheal signal) was mostly detected along stretches of C4 da neuron dendrites close to or within the Mav expression domain. Scale bars, 10 µm. (C and D) Stochastic Gal4 expression (*actin- > FRT > y+ > FRT > Gal4*) using epithelium-specific Flp lines with (C) low (LF-Flp) or (D) high (HF-Flp) activity in combination with

up- (*mav*^{OE}) or downregulation (*mav*^{RNAi}) of Mav. Epithelial clones (labeled by GFP) and C4 da neurons (*ppk-CD4-tdTomato*) were visualized in third-instar larvae. Scale bars, 100 μm.

(E) Quantification of C4da neuron dendrite length covering GFP-expressing epithelial cells (indicated in green) and surrounding areas (indicated by a red-shaded region surrounding GFP-labeled epithelial cells). *Mav*^{OE} promotes dendrite coverage of GFP-positive epithelial cells and surrounding areas. *Mav*^{RNAi} in few cells (LF-Flp) results in local reduction of dendrite coverage on GFP-positive epithelial cells (n = 29, 33, 27, 29, 33, and 27 cells from n = 5 animals per genotype, mean ± SD, one-way ANOVA, Bonferroni *post hoc* test, *p < 0.05, **p < 0.01, ***p < 0.001).

(F) Quantification of C4da neuron dendrite length covering GFP-labeled (HF-Flp > *mav*^{RNAi}, indicated in green) or non-expressing epithelial cells (indicated in red). Reduction of Mav levels significantly reduces dendrite coverage of GFP-expressing and non-expressing cells (red shaded areas in D; n = 20, 15, 20, and 15; mean ± SD; oneway ANOVA; Bonferroni *post hoc* test; *p < 0.005, ** p < 0.001).

Center lines of boxes represent median values; small squares are average values; upper and lower edges of the boxes represent the 75th and 25th percentiles of the sample data, respectively; whiskers represent 95th and 5th percentiles of the sample data.